



# Interfacial Velocities During Dynamic Imbibition

Graduation Project in Applied Physics



Name  
Students number  
University, study  
Class  
Period  
Submission date

T.J.J. van Beusekom (Tom)  
09015361  
The Hague University, Applied Physics  
NH4  
26-08-2013/18-12-2013  
18-12-2013

Company  
Department  
Internship supervisor  
Professor  
Professor  
External

Shell Global Solutions International BV  
Rock and Fluid Science  
dhr. R.T. Armstrong  
mw. drs. M.C. Vloemans  
dhr dr. ir. C.A. Swarts  
dhr. J. Mes



# **Interfacial Velocities During Dynamic Imbibition**

Graduation Project in Applied Physics



## Abstract

Increasing oil and energy demand asks for a higher efficiency when it comes to oil recovery. In order to increase oil recovery efficiency, pore-scale mechanisms during waterflooding, a common recovery method, have to be better understood. This provides knowledge on the *dynamic* process during imbibition, which is currently lacking.

To gain more insight on these pore-scale mechanisms, experiments were conducted to capture pore-scale events during dynamic imbibition. The experimental setup consists out of a transparent glass micromodel, a high speed camera, and a transmission microscope. A high speed camera is used because it allows better mapping of the dynamic process than conventional cameras. Imbibition is carried out with water as wetting phase and air as non-wetting phase. The micromodel represents a porous rock and contains interconnected pores-bodies with a diameter of 60  $\mu\text{m}$ . The pore-necks are 13  $\mu\text{m}$  wide and 20  $\mu\text{m}$  long. The depth of the model is 10  $\mu\text{m}$ . The model's wetting state is water-wet with a contact angle of  $(19 \pm 3)^\circ$ .

The main point of the investigation is the dependency of interfacial dynamics on bulk flowrate. Flowrates of 1 nl/min up to 320  $\mu\text{l}/\text{min}$  were tested, corresponds to capillary numbers of  $9,19 \cdot 10^{-10}$  to  $2,94 \cdot 10^{-4}$ . Average front displacement is in range of 0,57 m/day to 18 km/day. Tests on front velocities in the order of 0,6 m/day are field relevant, higher front velocities are only investigated for understanding of interfacial dynamics. Interfacial velocities were determined by measuring displacement of the three phase (air, water, and glass) contact point in the captured video images.

Immiscible displacement in porous media is characterized by capillary number and mobility ratio. Capillary number stands for the competition between viscous and capillary forces. Viscous forces are induced by injection of fluid, and capillary forces by the capillary effect. As long as interfacial velocity increases with injection flowrate, viscous forces dominate displacement. As capillary forces dominate displacement, interfacial dynamics are independent of injection.

No dependency of interracial velocity on the bulk flowrate was observed for flowrates in range of 1 nl/min to 10  $\mu\text{l}/\text{min}$ , indicating that the system is capillary dominated. For flowrates corresponding to front velocities of 5,8 and 18 km/day an increase in injection resulted in a higher interfacial velocity, indicating that viscous forces start to play a role in the displacement. This conclusion is supported by the event flowrate, the rate at which an interface displaces air. Again no dependency is found on injection flowrate. When the ratio of event flowrate to injection flowrate is examined, it is found that viscous forces start to play a role in displacement as injection exceeds 10  $\mu\text{l}/\text{min}$ . This conclusion is supported by visual observation of the displacement front

To investigate influence of wettability on interfacial velocity, dynamic imbibition experiments were carried out on an intermediate wet micromodel with a contact angle of  $(90 \pm 4)^\circ$  at an injection flowrate of 100 nl/min. Measurements indicate that a larger contact angle, compared to a water-wet case, leads to lower interfacial velocity. An explanation is found by considering capillary pressure, which goes to 0 as the contact angle approaches  $90^\circ$ . With decreasing capillary pressure, displacement will be less capillary dominated and more viscous dominated.



## **Preface**

This report concerns the seventeen week graduation project at Shell Global Solutions BV. The project was performed in the Rock- and Fluid Science department in Rijswijk, The Netherlands.

I applied of a graduation project at Shell, because they provide a good environment in which performing experiments is among the daily activities. Just because of that the support of the colleagues is outstanding. Furthermore, Shell is one of the biggest companies in the world, and therefore it is very interesting to see how a company of such scale is managed.

Specific interest goes out to the Rock and Fluid Science department because the sphere of action is interesting. Experiments are done to better understand the behaviour of oil fields. In the future, knowledge gained by these experiments will be used to support decision making in the field. It is nice to contribute to that (if only for a really small part) and also see how that is done in a global company.

Tom van Beusekom



## Evaluation of assignment by company supervisor

Student's name	T.J.J. van Beusekom (Tom)
Student's study	Applied Physics
Company name	Shell Global Solutions International BV
Company supervisor's name	R.T. Armstrong (Ryan)

### Question 1

*What is your judgement on the student's performance during the graduation period?*

Please use the following grades:

O = unsatisfactory; T = doubtful; V = satisfactory; G = good; U = excellent

	O	T	V	G	U
Initiative					×
Systematic approach					×
Quality of data collection					×
Quality (interim) report				×	
Theoretical knowledge				×	
Practical insight					×
Attention to detail					×
Attitude and behaviour					×
Independence					×
Speed of (quality)work					×
<b>Total evaluation of graduation assignment</b>					×

## Question 2

Was the graduation assignment of use to your company?

hardly  somewhat  yes

## Question 3

Are you willing to take part in another graduation assignment of the TIS Delft next year?

yes  no

If yes, will this be in the spring semester, the autumn semester or both?

spring  autumn  both

## Question 4

If you have any general comments on the student, the graduation assignment or the TIS Delft in general, state them below.

*Tom's performance during his internship was excellent. He was very independent and was able to deliver high quality data even though I was out of the office for a large fraction of the internship. He took the initiative to self educate through the Shell library and was always willing to discuss the fundamental concepts. I gave a slightly lower, but still good, score for the report quality and theoretical knowledge not because of a lack of communication skills nor understanding but because the topic is very challenging and thus a full understanding of the theoretical knowledge would require significantly more time. The project was indeed fundamental research with an open-ended set of objective. I believe Tom handled this level of uncertainty well and is very deserving of an overall score of excellent.*

*As a side note, we will indeed use the data that Tom collected during his internship as part of the ongoing digital rock research at Shell. And we are very pleased to have this dataset for the testing of numerical pore-scale models.*

Date: 18-12-2013

Date: 18-12-2013

For approval company supervisor:

Seen by student:



R.T. Armstrong (Ryan)

T.J.J. van Beusekom

Shell Global Solutions International BV

Student The Hague University





# Table of Contents

1	Introduction.....	1
2	Oil recovery .....	3
2.1	Sedimentary rock.....	3
2.2	Oil reservoirs.....	3
2.3	Primary oil recovery.....	4
2.4	Secondary oil recovery.....	4
2.4.1	Waterflooding.....	5
2.5	Tertiary oil recovery or Enhance Oil Recovery.....	5
3	Physical background.....	7
3.1	Interfaces and interfacial tension.....	7
3.2	Contact angle.....	8
3.3	Capillary bundle model.....	10
3.4	Wettability.....	10
3.5	Waterflooding efficiency.....	11
3.6	Young-Laplace equation.....	12
3.7	Capillary pressure.....	13
3.8	Capillary rise.....	13
3.8.1	Washburn's equation.....	14
3.8.2	Darcy's law.....	15
3.9	Displacement mechanisms.....	16
4	Materials and methods.....	19
4.1	Experimental setup.....	19
4.2	Micromodel.....	19
4.3	Method on making pore-scale video images.....	21
4.4	Data processing.....	23
4.4.1	Interfacial velocity.....	23
4.4.2	Event flowrate.....	24
4.4.3	Fluid-fluid interfacial area.....	25
4.4.4	Wettability.....	26
5	Measurements and calculations.....	27
5.1	Types of events.....	27
5.1.1	C-events.....	27

5.1.2	E-events .....	27
5.1.3	W-events .....	28
5.2	Interfacial velocity .....	28
5.3	Event flowrate.....	30
5.4	Fluid-fluid interfacial area.....	31
5.5	Wettability.....	32
6	Results and discussions .....	33
6.1	Event hierarchy.....	33
6.2	Interfacial velocity .....	34
6.3	Event flowrate.....	36
6.4	Interfacial area.....	39
6.5	Wettability.....	40
6.6	Macroscopic displacement front.....	41
7	Conclusions.....	44
8	Future work .....	46
9	Acknowledgments .....	48
10	Bibliography .....	50
	Appendices.....	54
	Appendix A: dimensions of glass micromodel.....	54
	Appendix B: screenshots event types.....	55
	Appendix C: interfacial velocities .....	56
	Appendix D: comparison interfacial velocity water-wet and intermediate-wet micromodel.....	59
	Appendix E: displacement front.....	60
	Appendix F: event flowrate .....	64
	Appendix G: original project description.....	65





# 1 Introduction

In a typical oil reservoir, oil is stored in porous rocks, meaning that the rock consists of interconnected void spaces in which oil, but also small amounts of water, is present. In the beginning of deployment natural pressure of the field pushes oil up via a production well. Eventually, reservoir pressure starts to drop and therefore production decreases. To maintain pressure and thus production often water is injected. This technical process is called “waterflooding”. During waterflooding, oil is displaced by a process termed “dynamic imbibition”.

On average 43% of the initial oil in place is recovered from a reservoir. This is a high number compared to the beginning of the century, but still the other 57% remains trapped in reservoir rocks. This raises two important questions: (1) why does oil remains trapped in the pore-space and (2) how can it be mobilized to recover it.

## Relevance worldwide

The importance of this project can be described by looking at the worldwide energy demand. The US Energy Information Administration (EIA) has presented a long term vision on energy. It provides an estimate on many aspects of energy, and also on the worldwide energy demand. According to this report, energy demand will increase by 56% between 2010 and 2040. More than 85% of this increase occurs among developing countries outside the OECD<sup>1</sup> and is driven by their strong economic growth and expanding population. In 2040 still 28% of the total world energy consumption will be supplied by liquid fuels, as one can see in Figure 1-1[1]. To meet this demand, production and the recovery factor from existing oil reservoirs must increase.

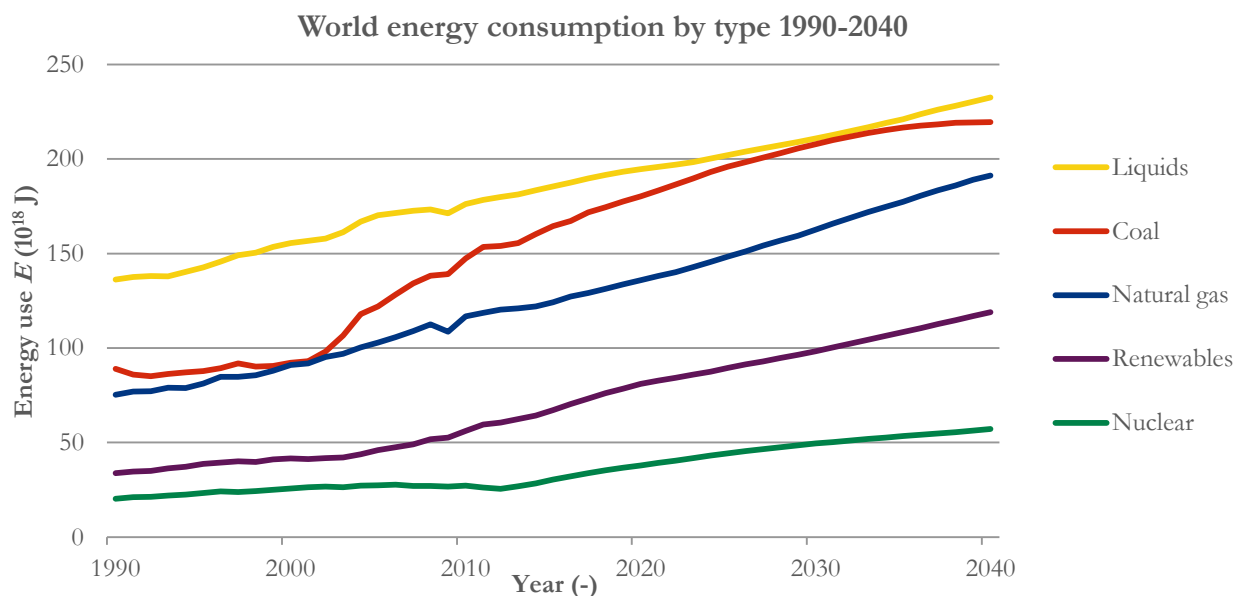


Figure 1-1. World energy consumption by type between 1990 and 2040 according to the projections of the EIA (U.S. Energy Information Administration), as presented in the “Long Term Energy Outlook” [1].

<sup>1</sup> OECD stands for “The Organisation for Economic Co-operation and Development”. Major members are US, UK, Canada, Japan, the Netherlands, and Germany. Major non-members are China and India.

## Objectives of the project

During dynamic imbibition, large fractions of the oil remain trapped in the pore-space due to many complex pore scale mechanisms. The effects of these pore-scale mechanisms play an important role on the macroscopic scale and thus on the amount of trapped oil. Many of these mechanisms have been investigated, but the data presented herein are unique in terms of the time and length scales at which the mechanisms are studied.

It is of crucial importance to understand the physics of imbibition to be able to increase efficiency of oil recovery. Currently there is a large interest in modelling multi-phase flow through a porous media directly on 3-dimensional digital images of a reservoir rock sample. This is often referred to as “Digital Rock”. To validate such simulations, experimental data are required for better understanding of pore-scale behaviour of oil displacement[2].

One approach on gaining a better understanding of pore-scale behaviour during dynamic imbibition, is performing experiments on a transparent micromodel, which gives a two dimensional representation of a porous rock. This micromodel consists of a network of interconnected pore-bodies which form a regular pattern. Together with a transmission microscope and a high speed camera direct visualisation of fluid motion is possible.

This leads to the following objectives for this project:

- I. *Produce pore-scale video images of pore-scale mechanisms during imbibition with a high speed camera.* Understanding the behaviour of dynamic imbibition starts with visualisation. From that point, observations and measurements can be done to work towards a conclusion.
- II. *Measure interfacial velocities at different flowrate.* A good parameter for the dynamics on the pore-scale is the velocity of the three phase contact point. This is the contact point between the wetting phase, non-wetting phase and the solid. Also the flowrate of the displaced phase will be considered during a single pore-event.
- III. *Evaluate if interfacial velocities are dependent on injection flowrate.* An important step in mapping dynamic imbibition, is determining whether interfacial velocities depend on injection flowrate or not.
- IV. *Investigate the influence of the wettability on the interfacial dynamics of the system.* The contact angle is a parameter characterizing wettability, it indicates whether the solid wants to be in contact with the wetting or the non-wetting phase. In the field the wettability of the porous rock can vary and therefore the influence of it on the interfacial dynamics will be investigated. In order to test wettability, experiments will be performed on both water-wet and intermediate-wet micromodels.

## 2 Oil recovery

A short background on oil and oil recovery is necessary to provide a view on the greater picture of this project, and will be given in this Chapter. Furthermore some terminology is provided to understand further technical explanations. The physical context will be provided in Chapter 3.

### 2.1 Sedimentary rock

The term petroleum is derived from the Latin words for rock (petra) and oil (oleum) and stands for a substance consisting of hydrocarbons found in rock formations, often sedimentary rock. Most petroleum was formed millions of years ago from organic matter, such as plants and animals buried under at least 1.5 m of sediments. These sediments prevent the organic matter from decomposition. Under the influence of high pressure and high temperature crude oil is formed from this organic matter. The same pressure and temperature that form oil from organic matter also, turn sediments into sedimentary rocks. These rock formations are porous, which means that oil can move throughout the rock. The void space in the sedimentary rock is called pore space, and is forming porosity. The degree in which oil can move through this pore space is given by the permeability, the amount of pore space is indicated by the porosity. A sample of a porous rock is shown in Figure 2-1[3].

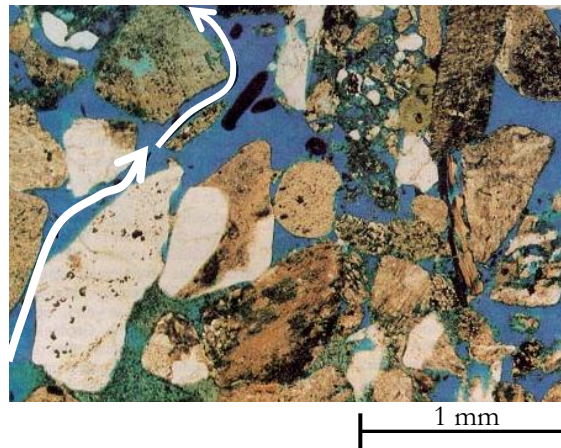


Figure 2-1. A magnified image of sandstone. The rock sample was injected with a blue-coloured epoxy. The interconnected blue areas indicate the pore space of the rock. The arrows in the figure show a possible path for oil flow[3].

### 2.2 Oil reservoirs

Crude oil is found in oil reservoirs. A reservoir is a subsurface body of rock which has a sufficient porosity and permeability to store and transmit oil. Sedimentary rocks are the most occurring reservoir rocks because they have a high porosity and are formed under temperature and pressure conditions at which hydrocarbons can be preserved[4]. A cap rock is found on top of the reservoir and prevents crude oil from migrating beyond the reservoir. The cap rock is relatively impermeable for oil and gas. The situation as described is illustrated in the image in Figure 2-2[5].

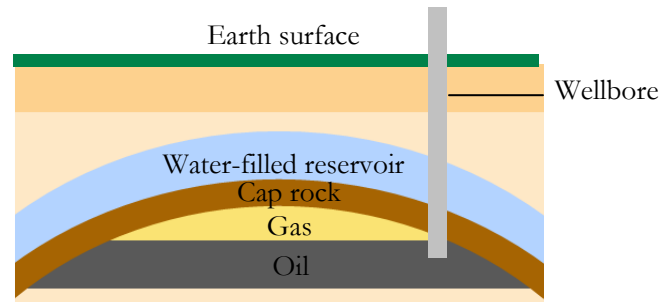


Figure 2-2. A cross section through a hydrocarbon reservoir. A cap rock prevents gas and oil from leaving the reservoir. Via the wellbore gas and oil is recovered [5].

Before any processing of oil can be done, it has to be recovered. Recovery methods are divided into three different types and are described in the next Sections.

### 2.3 Primary oil recovery

During the first stage of recovery, natural reservoir energy (i.e. pressure) displaces hydrocarbons from the reservoir into the wellbore and up to the surface. Driving energies can be gas-, or waterdrive or gravity drainage. In gasdrive the free gas, as displayed yellow in Figure 2-2, expands and drives the oil from the reservoir into the wellbore. Basically, the same happens in waterdrive, where water from any kind of source pushes oil into the wellbore from bottom down. Initially the pressure in the reservoir is higher than the pressure in the wellbore; so a pressure differential exists. Therefore, oil moves to the surface without the need for pumping.

As the reservoir pressure decreases, the production decreases as well because a lower pressure gradient results in a lower flowrate. At a certain point, it is necessary to implement an artificial lift system, such as a rod pump or an electrical pump. During the primary stage of recovery only 10% of the initial hydrocarbons in place are produced. The next stage of production is secondary recovery[6].

### 2.4 Secondary oil recovery

During secondary recovery, an external fluid (e.g. water or gas) is injected into the reservoir through an injection well. The goal of secondary recovery is to maintain reservoir pressure. Pressure is needed to displace the hydrocarbons towards the wellbore. Common used techniques in secondary recovery are gas injection or waterflooding. The latter is related to this research project and will be discussed extensively in Section 2.4.1 Waterflooding. During gas injection gas is injected into the gas cap from Figure 2-2 to maintain pressure[7].

The secondary stage comes to an end when the injected fluid is produced from the wellbore in a significant amount. Together primary and secondary recovery methods produce about 45% to 50% of the original oil in place in most situations. Sometimes factors reach up to 60%[8].

### 2.4.1 Waterflooding

Waterflooding is a commonly used secondary oil recovery practice. During waterflooding oil is displaced by the process of dynamic imbibition. Imbibition is a process where the wetting phase displaces the non-wetting phase in porous media. The term “dynamic” indicates that the process is initiated by pumping. A wetting and a non-wetting fluid are immiscible and therefore form an interface. Types of interfaces that often occur in an oil field are oil/water, oil/gas, and water/gas[9]. The dynamics of these interfaces are what causing the trapping of residual oil, and thus the efficiency of waterflooding.

Figure 2-3 gives a two dimensional illustration of the dynamic imbibition process. A wetting phase is being injected at the injection well into a porous ground layer which contains oil. Water drives the oil in the porous rock towards a production well. At this well a pump brings a mixture of oil and the wetting phase to the surface.

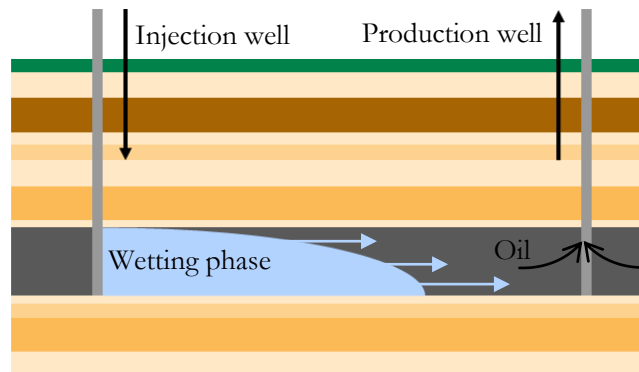


**Figure 2-3. A graphical representation of waterflooding. Water is being injected in the injection well. A wetting phase displaces oil that is stored in the porous media to a production well. Usually injection wells form a pattern around production wells[10].**

Note that in imbibition typically less than 50% of the non-wetting phase is displaced, due to capillary effects on the pore scale, which is the main topic of interest in this work.

### 2.5 Tertiary oil recovery or Enhance Oil Recovery

When water is produced in significant amounts at the production well, e.g. after breakthrough, tertiary recovery is needed. Sometimes tertiary recovery is indicated with the term Enhanced Oil Recovery (EOR). These practices can be more expensive, but are still profitable when the oil’s world market price is high enough. More effort is done to recover the oil and it also requires more processing after recovery[11].

After waterflooding, EOR techniques can recover an additional 7-15% on average[8]. EOR entails changing the actual properties of the hydrocarbons or the reservoir itself, which distinguishes this production phase from the previous two. While waterflooding and gas injection are used to push oil through the well, EOR applies steam or gas to change the makeup of the reservoir.



### 3 Physical background

This Chapter will give insight in the physical quantities relevant to multiphase flow through porous media. This includes the influence of surface tension, contact angle and viscosity on the system. Also the fundamentals of wettability and capillary pressure will be discussed. At the end of this Chapter, efficiency of dynamic imbibition is explained.

#### 3.1 Interfaces and interfacial tension

During imbibition a wetting phase is used to displace a non-wetting phase inside the pores of porous rocks. The fluids do not mix, and therefore an interface exists in-between the two phases. For convenience, an interface can be conceptualized as a layer with no thickness which separates the fluids.

When looking at the water-air interface for example, two different “types” of water molecules can be distinguished. Interior molecules are located inside the bulk volume and exterior molecules are located at the interface between water and a second fluid. Interior molecules are attracted to all surrounding molecules evenly; therefore their energy state is low. Exterior water molecules experience attractive forces from interior and neighbour molecules, but not from molecules from the other fluid. This causes surface molecules to miss half of the attractive interactions, which means that the liquid molecule is in an unfavourable energy state: unbalanced forces lead to additional energy. This provides the reason why that liquid form spherical shapes that minimize the overall surface area[12]. The described situation is illustrated in Figure 3-1. Surface energy of a material is the excess energy per unit area due to the existence of the free surface.

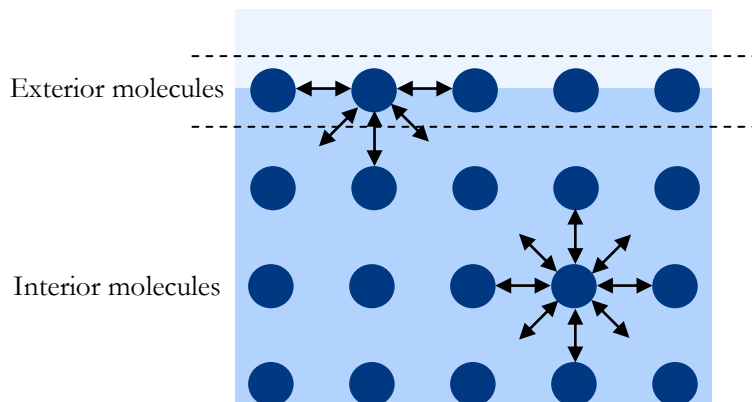


Figure 3-1. A simplification of a fluid-fluid interface. Attractive forces are represented by the black arrows. Molecules at the surface are missing half of the attractive forces compared to bulk molecules. Surface molecules are in an unfavourable state and therefore liquid adjust their shape in order to expose the smallest possible surface area [13].

To provide a more strict definition of surface tension Figure 3-2 A is considered. An arbitrary line  $AB$  separates fluid 1 from fluid 2. Across an element  $\delta l$  region 2 exerts a force  $F$  tangential to the surface. The magnitude depends on the interfacial tension  $\sigma$ . In Figure 3-2 B, a spherical cap is considered. This cap is

subjected to the surface tension around the base of the cap and to pressure  $P'$  and  $P''$ . The effect of the surface tension is to reduce the size of the sphere, unless it is opposed by a sufficiently great difference between pressure  $P''$  and  $P'$ .

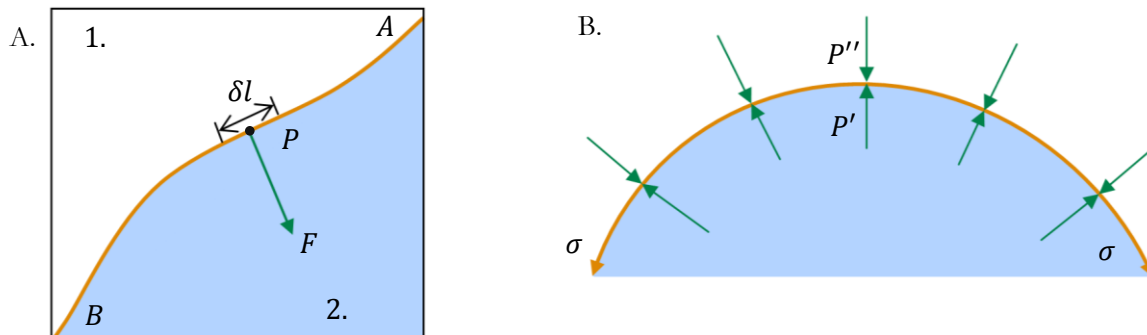


Figure 3-2. A: definition of interfacial tension at a point  $P$  on a line  $AB$ . B: capillary equilibrium of a spherical cap[14].

The force exerted from surface 1 to 2 can be calculated with equation (3-1)[14]:

$$F = \sigma \delta l \quad (3-1)$$

in which:

$F$	force from surface 1 to 2	[N]
$\sigma$	interfacial tension	[N/m]
$\delta l$	length of the element	[m].

In general, a decrease in the interfacial tension causes the permeability of the displaced phase (oil) to increase more than that of the displacing phase (water). This means that recovery efficiency of oil in porous media increases as interfacial tension decreases[15].

### 3.2 Contact angle

In any imbibition process in a porous media three phases are involved: one solid phase (porous medium) and two immiscible fluid phases. In the presence of three phases the following interfaces are present: solid-liquid, solid-gas, and gas-liquid. These interfaces are all subjected to surface tension and meet in one point. At this point three surface forces act, and depending on the magnitude of these forces the solid and fluids meet at a certain angle. This angle is called the contact angle.

Figure 3-3 illustrates three situations, which can be physically described by Young's Equation. This equation describes the relation between the interfacial tensions and the contact angle, and is stated in equation (3-2):

$$\sigma_{lg} \cdot \cos \theta_c = \sigma_{sg} - \sigma_{sl} \quad (3-2)$$

in which:

$\sigma_{lg}$	interfacial tension between liquid and gas phase	[N/m]
$\theta_c$	contact angle	[–]

$\sigma_{sg}$	interfacial tension between solid and gas phase	[N/m]
$\sigma_{sl}$	interfacial tension between solid and liquid phase	[N/m].

Note that contact angle is a static condition, and therefore it is calculated by a force balance: the sum of all surface forces has to be equal to zero, just as is stated by Young's equation.

In the left situation in Figure 3-3 the contact angle is smaller than  $90^\circ$ . This indicates that the solid surface is so called water-wet, the wetting phase has a tendency to spread over the surface, resulting in a relatively small angle. On the right an opposite situation is depicted. Here the contact angle is bigger than  $90^\circ$ , due to high surface force acting between the solid and the liquid. This is a so called oil-wet situation. An intermediate-wet situation is found in the middle, the contact angle is at or near  $90^\circ$ . With this example the term wettability is introduced. How wettability influences waterflooding performance is explained in the next Section.

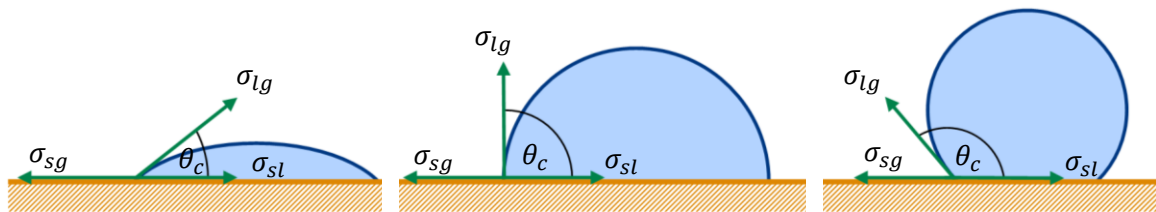


Figure 3-3. Different situations of contact angle: a water drop (blue) is applied on a solid surface (orange), depending on surface forces a different contact angle exists. [16].

If a surface is rough, Young's Equation is applicable to each element of the surface, causing that an apparent contact angle differs from the actual contact angle, as illustrated in Figure 3-4. Water droplet 1 (blue) wets a rough surface (orange). Due to the roughness the apparent contact angle (as measured from the apparent surface) is somewhat larger than  $90^\circ$ , while the actual contact angle (as measured from the actual surface) is somewhat larger than  $45^\circ$ . The situation as described could also occur as indicated by water droplet 2, when the apparent contact angle is much smaller than the actual contact angle [17].

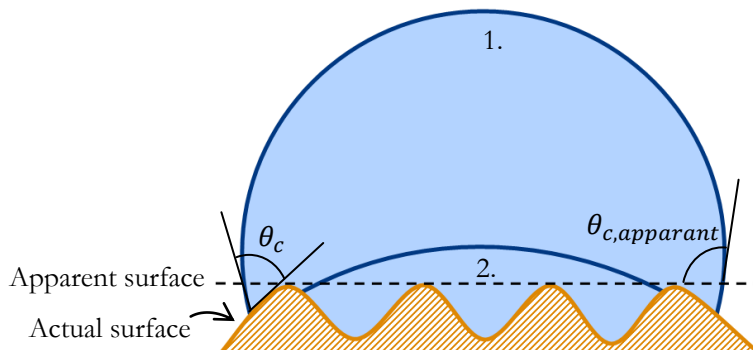
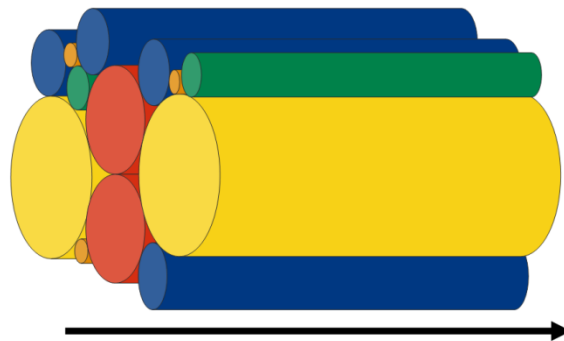


Figure 3-4. The effect of surface roughness on apparent contact angle,  $\theta_{c,apparent}$ . Due to the rough surface the contact angle and the apparent contact angle differ [17].

This phenomenon has to be taken into account when studying contact angles, certainly when the contact angle appears at a sharp corner. Glass itself has a really smooth surface, but at corners some roughness may have influence on the contact angle.

### 3.3 Capillary bundle model

Often porous media are visualized as a bundle of capillaries. The capillaries have a distribution in diameter. When looking at this model, some phenomena experienced during waterflooding can be described. Figure 3-5 provides an example of a bundle of capillaries.



**Figure 3-5. A bundle of capillaries with a distribution in diameter. The black arrow indicates the flow direction (horizontal).**

When looking at capillary invasion, the fact is known that, for a given range of diameters, small capillaries are invaded faster than larger ones (i.e. before hydraulic conductivity plays a role. This due to the higher capillary pressure in smaller tubes (diameter and thus the cross section is stated in the denominator). So when the left end of the bundle of capillaries is exposed to water, it penetrates the small capillaries at a higher rate than large ones. This causes the water to move ahead of the bulk water and is also known as corner-flow. During waterflooding corner-flow also takes place, where water advances ahead of the displacement front. This is also known as capillary fingering, as explained in Section 3.9 Displacement mechanisms. Now, water is pumped in the bundle and because of Darcy's law a higher volume flux is allowed in large capillaries (see Section 3.8.2). This allows the displacement front to catch up the corner-flow.

### 3.4 Wettability

Reservoir rocks are complex structures, and often comprise a variety of mineral types. Each mineral has a different wettability resulting in several types of wettability distinguished on the macro-scale: water-wet, oil-wet, intermediate-wet (lacking of a strong wetting preference) and mixed-wetting (having variety of wetting preferences). Figure 3-6 displays the influence of types of wettability on the spatial arrangement of oil and water at the pore-scale.

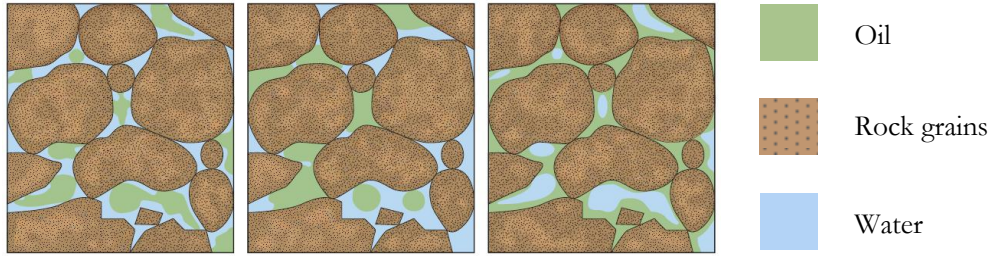


**Figure 3-6. The influence of wettability on spatial arrangement in porous media. All three conditions have a similar water and oil saturation. In a water-wet situation (left) oil remains in the centre of the pore-body. The reversed condition holds if surfaces are oil-wet (right). In the mixed-wet case (middle), oil has displaced water from some of the surfaces, but is still in the centres of water-wet pores[16].**

Thus, wettability describes the preference of a solid to be in contact with one fluid rather than another. Relating this to contact angle it is clear that a small contact angle leads to water-wet rocks where water is forming a film around the grains. Oil is present in the pore space. The other outer situation is a large contact angle, where oil is forming a film around the grains and water is trapped in the pore space[16].

### **3.5 Waterflooding efficiency**

In water wet formations, oil remains in the larger pores, where it can be snapped off by corner flow, or become disconnected from a continuous mass of oil, and become trapped. In an oil-wet or mixed-wet formation, oil adheres to surfaces, increasing the possibility of a continuous path to a producing well, and resulting in lower residual oil saturation. Imbibition forces – the tendency of a formation to draw in the wetting phase – determines how easily water can be injected and how it moves through a water-wet formation. Water breakthrough occurs later in a waterflood, and more oil is produced before water breaks through in a water-wet reservoir than in an oil-wet reservoir. The capillary entry pressure in this geometry relates to the inscribed radius of the largest adjacent pore throat. Although most of the pore bodies may fill with oil, the inter-space where grains meet do not fill, because the capillary pressure is insufficient to force the nonwetting oil phase into those spaces.

Most rock formations in practice are intermediate-wet or oil-wet. A decrease in wettability is reflected by an increase in the water permeability and a decrease in oil permeability. In the oil-wet rock, oil displacement continues after many pore volumes<sup>2</sup> (PV's) have been injected, while in the water-wet rock, the process is completed for all practical purposes within a few PV's. In general, residual oil saturation in uniformly wetted porous media is greater when the rock is strongly oil-wet. This means that displacement will occur at a slower rate and probably at lower efficiency in a strongly oil-wet reservoir. Reversely, water-wet rock formations lead to a higher efficiency in oil recovery [15]. This means that wettability is of great influence on the efficiency of waterflooding.

<sup>2</sup> Pore-volume: the total volume within a porous rock that can contain liquid[37].

### 3.6 Young-Laplace equation

Interfacial tension gives rise to a pressure difference across a curved interface between two immiscible fluids. By the magnitude of this pressure difference the shape of the interface is determined. The Young-Laplace equation relates the curvature of an interface to the interfacial tension and the pressure difference.

Before going to the equation first the situation in Figure 3-7 is considered. An arbitrary surface is displayed. Due to surface tension the curvature is characterized by two principal radii. The pressure at the bottom side ( $P''$ ) is higher than at the top ( $P'$ ) and therefore the surface curves upwards. The curvature as displayed is in equilibrium state.

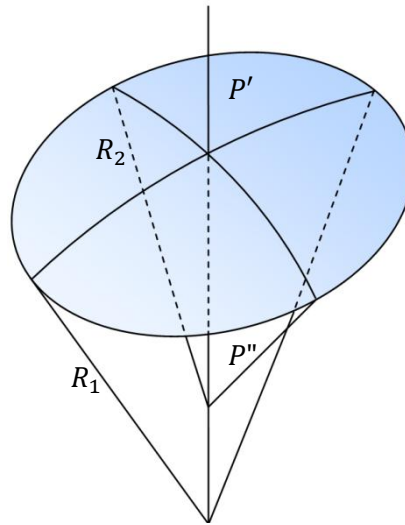


Figure 3-7. Capillary equilibrium of a non-spherical cap [14].

The relation between increased pressure on the concave side of a meniscus, the radii of curvature, and surface tension is given by equation (3-3):

$$P'' - P' = \sigma \left( \frac{1}{R_1} + \frac{1}{R_2} \right) \quad (3-3)$$

in which:

$P''$	pressure on the concave side	[N/m <sup>2</sup> ]
$P'$	pressure on the convex side	[N/m <sup>2</sup> ]
$R_1$	radius of curvature in $x$ -direction	[m]
$R_2$	radius of curvature in $y$ -direction	[m].

In case when applies that  $R_1 \approx R_2$ , equation (3-3) will turn into equation (3-4)[18]:

$$P'' - P' = \frac{2\sigma}{R_m} \quad (3-4)$$

in which:

$R_m$	mean radius of curvature	[m].
-------	--------------------------	------

The curved interface as described in the Young-Laplace equations introduces the next subject: capillary pressure.

### 3.7 Capillary pressure

For a single interface the capillary pressure is defined as the pressure difference across a curved interface, for example the interface displayed in Figure 3-7. Porous media are often visualized as a bundle of capillaries with a distribution of body size and capillary radius. Each capillary is invaded by a nonwetting oil phase at a different capillary entry pressure, which is inversely proportional to that capillary's radius, as becomes clear from equation (3-5):

$$P_c = P'' - P' = P_{nonwet} - P_{wet} = \frac{2\sigma \cdot \cos \theta_c}{a} \quad (3-5)$$

in which:

$P_c$	capillary pressure	[N/m <sup>2</sup> ]
$P_{nonwet}$	pressure inside the nonwetting phase	[N/m <sup>2</sup> ]
$P_{wet}$	pressure inside the wetting phase	[N/m <sup>2</sup> ]
$a$	diameter of the individual capillary	[m].

In dynamic imbibition a wetting phase (water) displaces a non-wetting phase (oil). In order to do so, the pressure in the wetting phase has to increase, since initially the pressure in non-wetting phase is higher than the pressure of the wetting phase. Thus, oil will be displaced spontaneously from a tube if the pressure in the oil phase is reduced, even though the pressure in the water phase is still less than the pressure in the oil phase [19, 20].

Also the contact angle is of influence on the capillary pressure. At an angle of  $\theta_c=90^\circ$  the capillary pressure will be zero, because the interface is flat (and of course because  $\cos(90^\circ)=0$ ). A smaller contact angle will bend the interface down, resulting in a local lower pressure on the convex side.

### 3.8 Capillary rise

Capillary pressure is the pressure difference between the wetting and the non-wetting phase. This phenomenon initiates a capillary rise in small capillaries, as depicted in Figure 3-8. The phenomenon of capillary rise is important to understand because, as explained in Section 3.3, a porous medium is often described in terms of a bundle of capillary tubes.

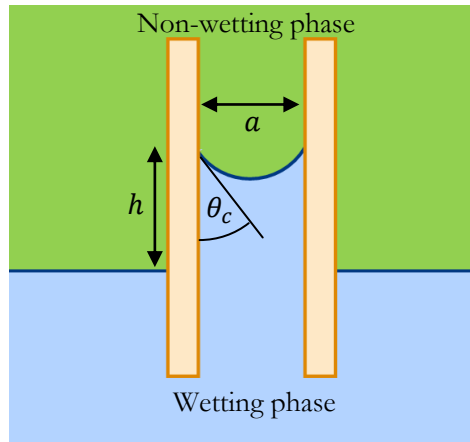


**Figure 3-8.** The classical example of capillary rise. A small water-wet capillary is inserted into a liquid. The liquid level in the capillary rises above the liquid level outside the capillary.

The curved interface will rise until the following applies:  $P_c = \rho g h$ . More on this topic will be explained in the next Sections.

### 3.8.1 Washburn's equation

Capillary pressure causes a wetting phase to spontaneously enter ('imbibe') a narrow capillary. The rate of penetration into this small horizontal capillary is described by The Washburn Equation, as displayed in equation (3-6):

$$\frac{dl}{dt} = \frac{r}{\mu} \cdot \frac{\sigma}{4l} \cdot \cos \theta_c \quad (3-6)$$

in which:

$\frac{dl}{dt}$	penetration rate into capillary	[m/s]
$r$	diameter of the capillary	[m]
$\mu$	viscosity of the displacing phase	[N · s/m <sup>2</sup> ]
$t$	time	[s]
$l$	travelled distance in porous media	[m].

In words this equation means that the rate at which a liquid penetrates a horizontal capillary under its own capillary pressure is directly proportional to the radius of the capillary, to the cosine of the contact angle, the ratio of the surface tension to the viscosity of the liquid and inversely proportional to the length already filled by the liquid [21]. A few assumptions were made, so these have to be taken into account when applying this equation to a practical situation. It is assumed that there is no resistance of the displaced air and that the interface moves under its own capillary pressure. The latter is not exactly the case because injection of a wetting phase will build up pressure.

In the introduction the term "interfacial velocity" was introduced. Interfacial velocity is used to indicate the speed at which local (on the single pore-scale) displacement of the air-water interface take place. When looking at the dynamic imbibition process in the micromodel, interfacial velocity is defined as the velocity of the three phase contact point, i.e. where water, air, and the micromodel meet.

### 3.8.2 Darcy's law

When looking at flow through a macroscopic porous medium Darcy's law relates pressure gradient to flow according to equation (3-7):

$$Q = -\frac{kA}{\mu} \cdot \frac{P_e - P_b}{L} \quad (3-7)$$

in which:

$Q$	flowrate	$[\text{m}^3/\text{s}]$
$k$	permeability	$[\text{m}^2]$
$A$	cross section of the capillary	$[\text{m}^2]$
$\mu$	viscosity of fluid	$[\text{N} \cdot \text{s}/\text{m}^2]$
$P_e$	pressure at the end of the capillary	$[\text{N}/\text{m}^2]$
$P_b$	pressure at the beginning of the capillary	$[\text{N}/\text{m}^2]$
$L$	length at over which the pressure drop is taking place	$[\text{N}]$ .

The coefficient  $k$  stands for the permeability and is a function of the geometrical structure of the porous medium. It is a measure for the size distribution of the pore-bodies and their connectivity, the degree to which pores and/or channels are interconnected. The better pore-bodies are interconnected, the higher the permeability is. The minus sign indicates that flow is going in direction from high to low pressure.

This law is derived from the Hagen-Poiseuille law, which relates flow through a single capillary to the pressure drop, its radius, and its length. When assuming that a porous medium can be represented by a bundle of capillaries with two diameters, Darcy's law is obtained by applying the law each individual capillary [22].

### 3.8.3 Darcy velocity

When a porous medium is described by a bundle of capillaries, it is possible to calculate the velocity of the displacement front on a macroscopic scale. This velocity is called the Darcy velocity and is displayed in equation (3-8):

$$v_{Darcy} = \frac{Q}{A} \quad (3-8)$$

in which:

$v_{Darcy}$	Darcy velocity	$[\text{m}/\text{s}]$ .
-------------	----------------	-------------------------

The Darcy velocity is often indicates as the front velocity in this report. The front velocity is the average velocity at which the displacement front moves through the porous pattern and can for instance be used to describe how many meters per day the displacement front travels. In the results and discussion section, the front velocity will be compared to the interfacial velocities.

### 3.9 Displacement mechanisms

When immiscible displacement in porous media is studied at the macroscopic scale, i.e. when Darcy's law applies, displacement can be divided into three mechanisms, characterized by two dimensionless numbers: capillary number and mobility ratio. The displacement mechanism gives an indication of the shape of the displacement front, i.e. the entire length across which the dynamic imbibition process takes place. The capillary number is the ratio of viscous to capillary forces, and this gives an indication which of the two forces is dominant. Capillary number is given by equation (3-9):

$$Ca = \frac{v_{Darcy}\mu}{\sigma} \quad (3-9)$$

in which:

$Ca$	capillary number	[-]
$v_{Darcy}$	Darcy velocity	[m/s]
$\mu$	viscosity of the displacing phase	[N · s/m <sup>2</sup> ]
$\sigma$	interfacial tension between both phases	[N/m].

A capillary number of 10<sup>-6</sup> is typically for flow through pores in an oil reservoir[23]. But capillary number depends on viscosity and interfacial tension, and these values differ for oil-water displacement and air-water displacement. Therefore a better estimate of relevant capillary numbers is obtained from the front velocity, which is ~0,3 m/day, resulting in a capillary number for air-water displacement in the order of 10<sup>-10</sup>.

The mobility ratio, or also called viscosity ratio, is the ratio between the viscosity of the displacing phase and the viscosity of the displaced phase and can be found in equation (3-10):

$$M = \frac{\mu_1}{\mu_2} \quad (3-10)$$

in which:

$M$	mobility ratio	[-]
$\mu_1$	viscosity of the displacing phase	[Pa · s]
$\mu_2$	viscosity of the displaced phase	[Pa · s].

Figure 3-9 illustrates the three displacement types as function of capillary number and mobility ratio. Boundaries of the regimes depend on pore morphology, so they are indicative: they show position of the regimes with respect to the others, but do not define the numeric boundary conditions. Within the transition zone the displacement types blend into a mixed style. For certain values of the capillary number either viscous or capillary forces dominate the displacement. Since water-air displacement is considered in all cases the mobility ratio has a constant value, represented by the dotted vertical line. With increasing flowrate, the capillary number increases, see equation (3-9), which is represented by the dotted horizontal lines. Experiments will be conducted at the crossing of the vertical and horizontal lines, indicated by the coloured dots.

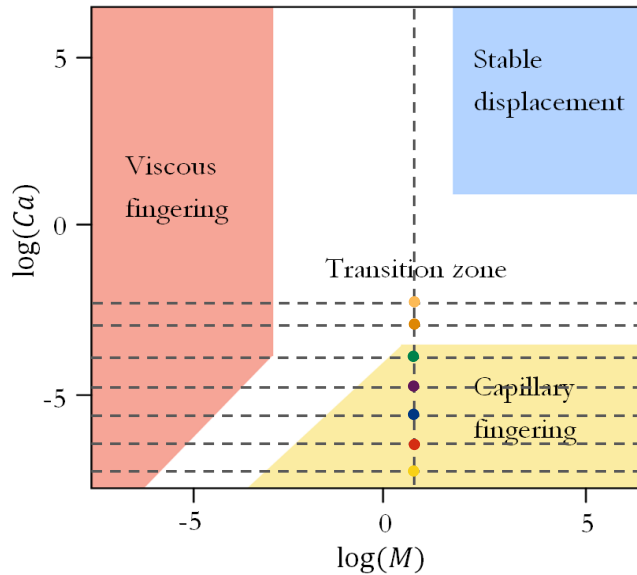
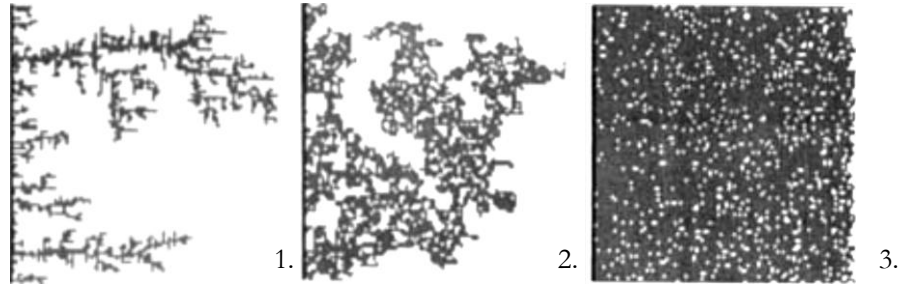


Figure 3-9. Schematic representation of two-phase fluid displacement types in porous media as a function of capillary number and mobility ratio. The dotted lines represent the capillary number (horizontal) and the mobility ratio (vertical). The first changes with flowrate and the latter is constant. Injection flowrates vary from 1 nl/min (yellow) to 320  $\mu$ l/min (light brown)[24].

Figure 3-9 was created by simulations by Lenormand[24] on a two-dimensional model of a porous rock. The model consisted out of 100 by 100 pores with a pore-body radius of  $r = 0.23$  mm. As show in Figure 3-9 displacement can take on of the following basic regimes:

1. *Viscous fingering* : in this regime capillary forces are negligible compared to the dominant viscous forces. Viscous fingering occurs at relatively high flowrates and when the displaced phase is more viscous than the displacing phase (i.e.  $M < 1$ ). Ahead of the displacement front treelike formations are formed. Once these formations have reached the other side of the model (breakthrough), almost all injected fluid moves via these so called “preferential paths”. This causes hardly any non-wetting phase displacement after breakthrough, and therefore this is an inefficient displacement regime.
2. *Capillary fingering* : this occurs at relatively low flow rates, where (due to capillarity) the wetting phase flows through the crevices of the pore-space. These fingers may grow in any direction, even backwards. They can form loops which trap the displaced fluid, leading to large residual oil saturation in practice. Capillary forces are dominant in this regime.
3. *Stable displacement* : stable displacement occurs at a relatively high flowrate and when the viscosity of the displacing phase is greater than the viscosity of the displaced phase (i.e.  $M > 1$ ). The pattern presents a flat front, with some irregularities at the scale of a single pore. The front remains flat because if a finger starts to form, the finger tip would have a lower pressure than the main front. Allowing the front to catch up. Stable displacement is the most efficient way of displacement through a porous rock when it comes to oil recovery. It limits the change of disconnecting a large area of oil [24].

Pictures of the displacement types as described above are displayed in Figure 3-10:



**Figure 3-10. Immiscible displacement can be divided in three types, as described by Lenormand: (1) viscous fingering, (2) capillary fingering, and (3) stable displacement. The displacing fluid is displayed black, the displaced fluid is displayed white [24].**

When relating this to waterflooding, the trapped displaced fluid represents oil. Knowing this, the preference of a displacement mechanism would obviously go out to stable displacement, because this results in the lowest residual oil saturation. For stable displacement a relatively high capillary number is needed. In practise this is hard to establish due to mechanical limitations, but also reservoir rock could fracture, resulting in large preferential paths.

Thus, behaviour of immiscible displacement on the macroscopic scale is widely investigated and therefore well understood. However, the dynamics of the different displacement types is only poorly understood and therefore is the main area of interest in this work. The focus in this report is on the dynamics of a single pore in a network of interconnected pore-bodies and pore-necks. Dynamics on the single pore will be compared to dynamics on macroscopic scale, i.e. front velocity versus interfacial velocity.

## 4 Materials and methods

This Chapter is dedicated to the experimental setup, which consists of many parts that will be described in the next Sections. All relevant technical details of the parts will be discussed. Also, methods for performing experiments are explained as well as the data processing procedure.

### 4.1 Experimental setup

Figure 4-1 gives a schematic view of the experimental setup. The setup consists of a micromodel, mounted in a holder and placed in a transmission microscope. MilliQ water is injected by a syringe pump and after it passed through the model it is drained to a waste container. While water passes the model, a high speed camera records images of the dynamic imbibition process.

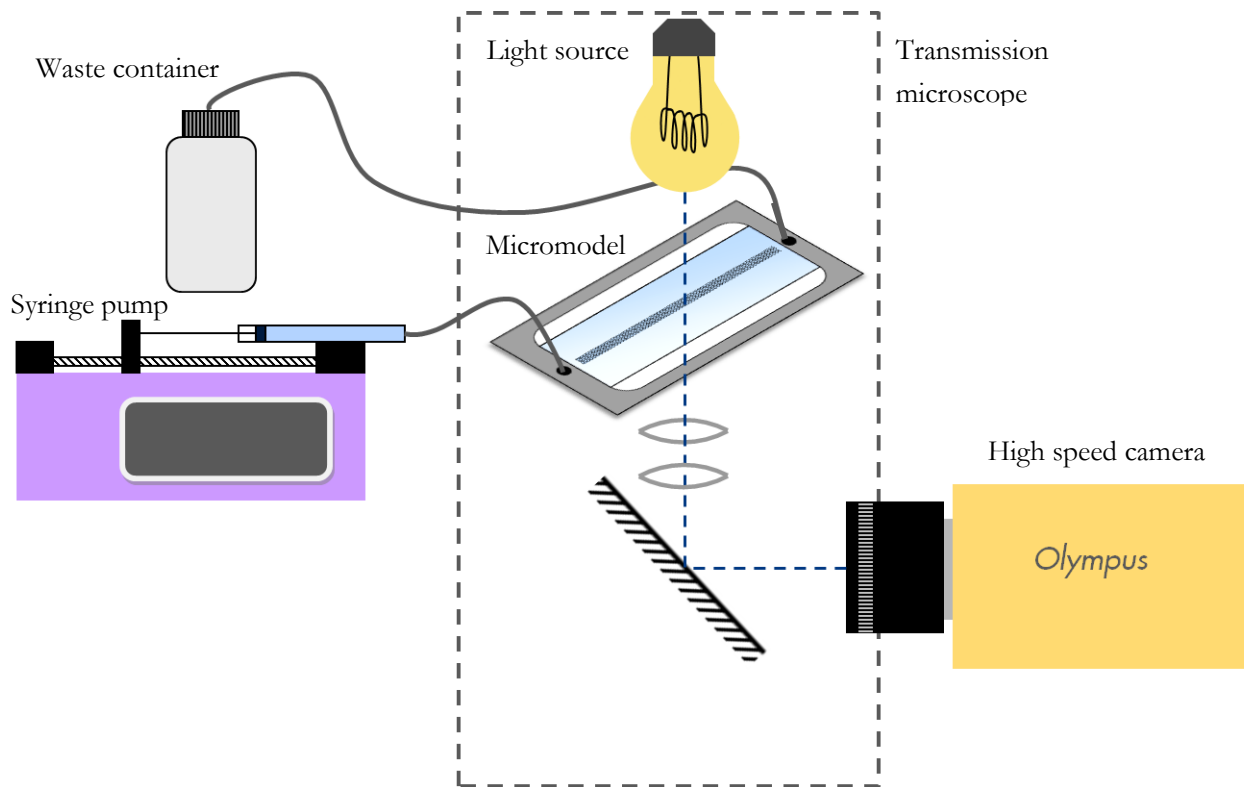
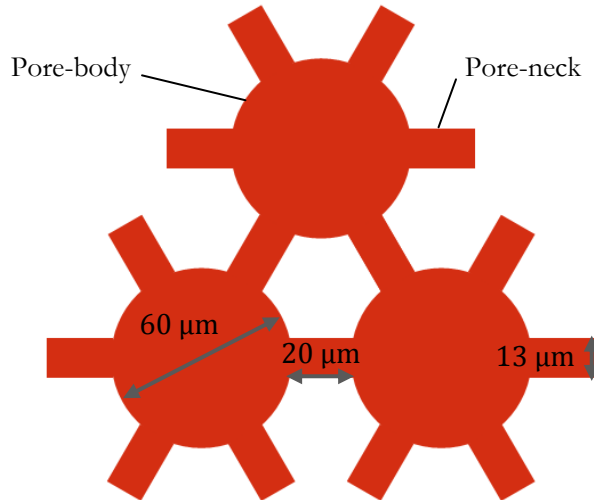


Figure 4-1. A schematic view of the experimental setup. The entire setup is placed on an optic table.

### 4.2 Micromodel

In this project a porous medium is represented by a two dimensional network of interconnect pores, chemically etched in Borosilicate glass. Because glass is used, direct visualisation by light microscopy is possible. In this regular, repetitive network pore-bodies are connected via pore-necks. The dimensions are chosen in a way that they represent common conventional reservoir rock. The pattern is five to six pores wide and 857 pores in length. Figure 4-2 shows dimensions of the pore-bodies and pore-necks.



**Figure 4-2. Pore-geometry is explained using three pores. Dimensions are shown in the figure. Depth of the channels is 10 μm. All given measures are theoretical values.**

The micromodel is delivered by Micronit, a commercial provider of micro-fluidic instrumentations, based on a design created by Shell. The network is chemical etched into the glass by using hydrofluoric acid. A mask is used for accurate positioning on the glass. Due to the chemical etching the design is limited to a 2:1 width to depth ratio which limits the depth. To create a model with the needed depth, two of the same plates are bonded together. This is done at very high temperatures, which makes the bond strong enough to hold up to 150 bar [25][26]. Figure 4-3 A shows a part of the micromodel pattern and B shows the complete micromodel.

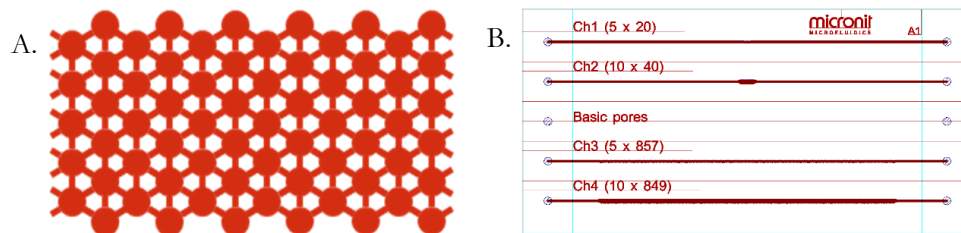


**Figure 4-3. A. Detail of the porous network. B. Complete micromodel with multiple channels, each with a different geometry.**

Chemical etching is a production procedure which leads to errors in the dimensions of the model up to 10%. The manufacturer has calibrated the actual measures of the two glass plates, and the result is displayed in Appendix A: dimensions of glass micromodel. Based on these numbers, dimensions with corresponding errors are determined and displayed in Table A1.

Imbibition is carried out with water as wetting phase and air as non-wetting phase. This is done because the micromodel is hard to clean due to the small pore structure. Demineralised water and a vacuum oven allows drying of the model by evaporation without any dry residue, which could influence the properties. Also, experiments can be done much quicker and more repeatable because the model is ready for use right after drying, instead of saturating the model with oil before experiments can be carried out. Water-air displacement

will be well comparable with water-oil systems because in both situations viscous and capillary forces are present. The main difference to oil-water is the much lower viscosity of air compared to oil, and the higher interfacial tension. Compressibility of air does not play a significant role.

Since wettability is also a point of interest, two wetting states of the micromodel will be investigated: a water-wet micromodel (WW), and an intermediate-wet model (IW). Tests on the WW model are used to determine interfacial velocity over a range of injection flowrates. Tests on the IW model are used for comparison between WW and IW model behaviour. A perfectly clean glass surface is water-wet [27], but any compound attached to the surface can influence wettability.

### **4.3 Method on making pore-scale video images**

To investigate interfacial velocity pore-scale video images of the imbibition process have to be made. The setup as displayed in Figure 4-1 is used. Imbibition is studied in which water is the wetting phase and air the non-wetting phase. Measurements will be conducted on an air saturated and water-wet micromodel.

Injection flowrates are varied from 1 nl/min to 320  $\mu\text{l}/\text{min}^3$ , and are varied with steps of one order of magnitude. Such small flowrates can be accomplished by a syringe pump. The type of the pump is Harvard Apparatus Picoplus, combined with a Hamilton 100  $\mu\text{l}$  syringe, type 1801 RN SYR. On the screen a certain injection rate can be selected, anywhere between pl/min to  $\mu\text{l}/\text{min}$ . The pump moves the piston of the syringe along a rotating screw thread. Images are recorded with a transmission microscope (Leica DMI6000B) and a high speed camera (Olympus i-SPEED 3). The camera is connected to the microscope via a F camera mount.

Experiments are conducted as follows:

1. The micromodel is placed in a holder. Via this holder the syringe and the waste container are connected to the model with plastic tubing.
2. The holder is mounted directly on the motorized stage of the microscope, which can move in two dimensions in the horizontal plane. Controlling of the stage is done by computer or focus wheel. As shown in Figure 4-1, a light bulb of 12 Volt is shining from above on the model. Intensity is adjustable in 20 steps and also a diaphragm is available for fine tuning of the light intensity.
3. After light passing through the model, it passes a lens. For this experiment the “10X” lens is used, which magnifies the beam by a factor ten. After passing the lens, the beam hits a mirror which reflects it to the horizontal direction and into the high speed camera.

Images are captured with the following procedure:

---

<sup>3</sup> Originally an injection flowrate of 1 ml/min would have been tested, but the maximum flowrate of the syringe pump was 320  $\mu\text{l}/\text{min}$ .

1. *Videos are recorded at 15.000 frames per second (fps).* The optimum frame rate is determined empirically, because it provided good images at a fair field of view<sup>4</sup>. To prevent blurring of the images the exposure time (1/15.000 s) is halved. In this way, one is still able to have a large and sharp image without any blurring. During recording an internal temporary memory is constantly rewritten. So when the meniscus has moved through the field of view the recording can be stopped. Approximately 5,6 s can be recorded at once. With bookmarks the relevant sections of the data can be select and transferred to a SD card. Figure 4-4 shows a typical screenshot from a video taken during the imbibition experiments. Explanation about the data processing procedure can be found in Section 4.4.

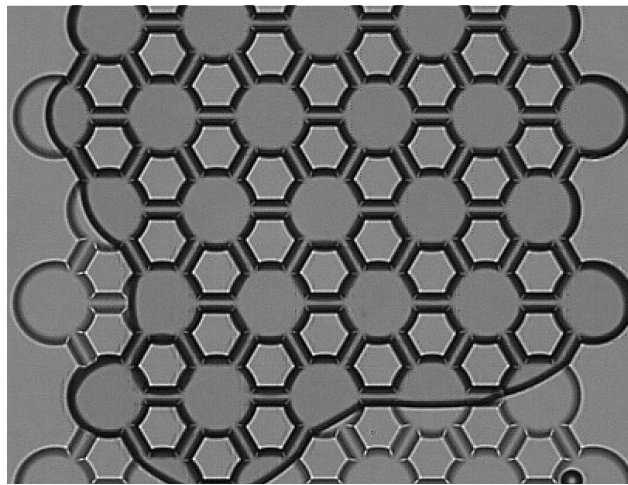


**Figure 4-4. A screenshot from a typical video image recorded during dynamic imbibition in the micromodel. The picture's dimensions are 432 pixels wide by 320 pixels high. Water is coming in from bottom up and is displayed lighter.**

2. *Water will be injected with the syringe pump into the micromodel.* The total internal volume of the pore-pattern is estimated to about 165 nl. Before water can enter the pore-pattern it has to travel along the feed channel, containing a relatively (compared to internal volume of the model) large volume of “dead space”. Injecting has to be carried out carefully, in order not to saturate the model at once. The dead space is estimated at 1900 nl. This volume is injected at a flowrate of 1  $\mu\text{l}/\text{min}$ .
3. *Videos are recorded from the passing of water through the pattern.* As shown in Figure 4-4 the field of view of the camera is about six by six pores. Recording start at the moment that water enters the screen and is stopped when it leaves.
4. *Models are put in the oven for drying.* This is done by a vacuum oven for at least 10 minutes. This allows evaporation of all water present in the model from usage. Since demineralised water is used, no residues are left after evaporation.

---

<sup>4</sup> A higher frame rate will lead to smaller images, since the camera is limited to a certain amount of data that can be processed per time unit. With a lower frame rate the advancement cannot be tracked because the distance travelled between two frames is too large.

For investigation on the influence of wettability, the IW model will be used. Experiments are performed as described above at a flowrate of 100 nl/min.

## 4.4 Data processing

Once the images have been recorded, data has to be extracted from the video images. Interest goes out to interfacial velocity, wettability of the micromodel, event flowrate, and interfacial area. In this Section explanation is given about how data is retrieved from the videos. Before any processing can be done, the captured videos have to be converted to a format which is accessible for the computer programmes used later on. This is done as listed below:

1. *Record video images.*

Images are recorded as described in Section 4.3.

2. *Convert images to avi.*

The file extension from data of the high speed camera is unknown to the data processing program. Therefore it has to be converted to an avi format on the computer using the manufacturer's software.

3. *Convert images to gif and tif format.*

An open source physics tool, called "Tracker", will be used to determine interfacial velocities. This program is only capable of processing gif images. Therefore the avi files have to be converted. The tif format images are created to view results back frame by frame, instead of as an animated gif image.

4. *Crop images to 150 by 150 pixels.*

Initially the image shows the entire field of view of about 6 by 6 pore-bodies. Interest only goes out to one pore-event at the time, so the avi files have to be cropped to show one pore-body and relevant adjacent pores. To execute this step the program "Image J" is used.

### 4.4.1 Interfacial velocity

First point of interest is the interfacial velocity. A video consist of a number of frames (pictures). With a given framerate the time between two frames is known. Interfacial velocity is determined by tracking the displacement of the three phase contact point between two frames, and dividing it by the timestep. This results in an average velocity at which that point has moved. The higher the framerate, the more precise the velocity profile can be described. The procedure for measuring interfacial velocity is as follows:

1. *Load gif images in Tracker.*

Gif images contain a sequence of frames, which all are loaded into Tracker.

2. *Calibrate images.*

First calibration has to be carried out to give in a length- and timescale. The length scale is defined by giving in a known distance, in this case the pore-body diameter. Timescale is set using the framerate in fps. This means that the time between two frames and the scale (in m/pixel) are known.

3. *Track three phase contact point.*

In the data processing procedure two three-phase contact points are tracked after splitting of an interface. In order to differentiate them, terms "point A" and "point B" are introduced. Splitting

always happens at a sharp corner of the glass model and therefore the lengths of the paths that yet have to be travelled are not equal. Point A refers to the point that has to travel the largest distance. Point B refers to the point that has to travel the smallest distance. Figure 4-5 shows a screenshot of the Tracker software and will explain more about determination of the velocity.

4. *Process data in Excel for further analysis.*

The result of the previous step is a large table with quantities like, time, velocity (in  $x$ -, and  $y$ -direction, and resulting), travelled distance, acceleration, etc.

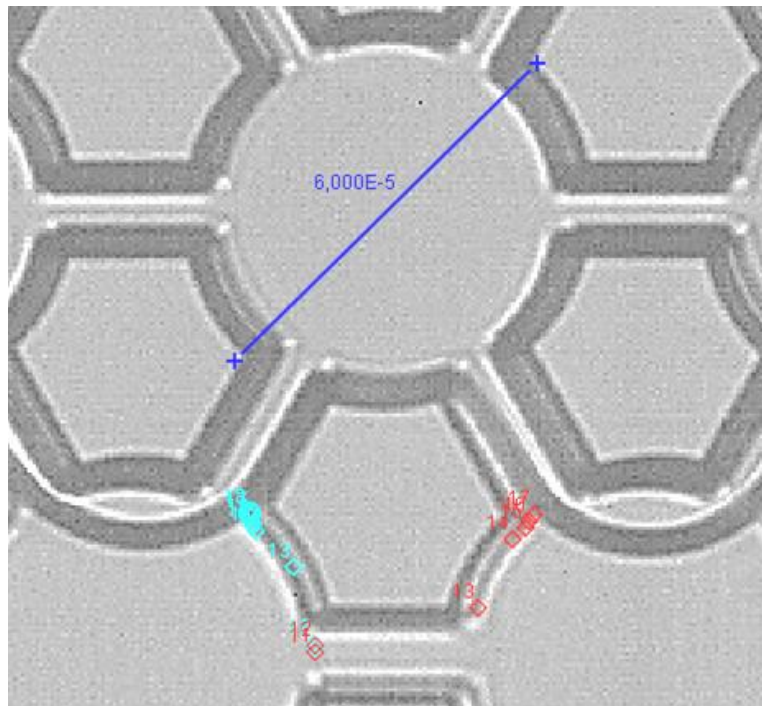


Figure 4-5. A screenshot of the data processing in Tracker. The blue line is used for scaling on the basis of the known diameter of a pore. The red (point A) and magenta (point B) dots are points where the three-phase contact point was located in different frames. The distance travelled in pixels is transferred to meters, which can be converted to a velocity in m/s, knowing the time between two frames.

5. *Plot data.*

Interfacial velocity is plotted as function of time.

#### 4.4.2 Event flowrate

The main question of this report is if, and to which extend, interfacial velocities depend on bulk flowrate. Since the interface moves through the micromodel during imbibition, air is displaced. Interest goes out to the rate at which air is displaced when a single event is examined, this is the so called “event flowrate”. Figure 4-6 provides explanation. Event flowrate is initiated by moving interfaces, so therefore it is interesting to see if interfacial behaviour is similar to behaviour of event flowrate, as injection flowrate is changed.

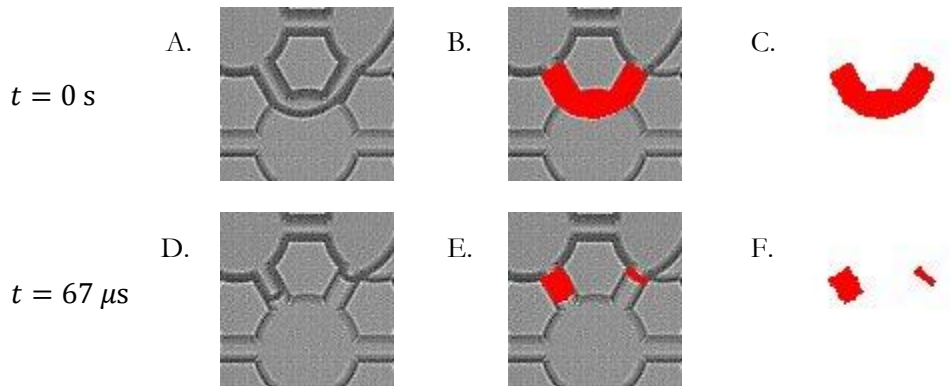


Figure 4-6. A single pore is displayed, water is coming from bottom up. As time progresses, air is pushed out of the pore-bodies via the pore-necks. Event flowrate is determined using two frames one time step after each other (A and D). The red marked areas mark the air present in the pore-necks (B and E). The area of B and E is calculated by counting pixels in pictures C and F (in red).

The difference in red area between Figure 4-6 C and Figure 4-6 F gives the area (in pixels) of the air that is displaced between the two time steps. The scale of the image (in  $m \setminus pixel$ ) is known from determine of the interfacial velocity. With the depth of the micromodel the displaced volume (in nl) can be calculated for comparison between injection flowrate and event flowrate. Since the time between the frames is known, even flowrate directly results from the displaced volume.

#### 4.4.3 Fluid-fluid interfacial area

During imbibition experiments water displaces air from the micromodel. Since the two fluids are immiscible an interface exists. Depending on the injection flowrate, the water-air interface has a certain shape with corresponding interfacial area. The interfacial area is the sum of all the separate fluid-fluid interfaces in individual pores. Interest goes out to how the total area of the interface alters as injection flowrate is changed. The interfacial area is determined in Avizo (image processing software), as displayed in Figure 4-7.

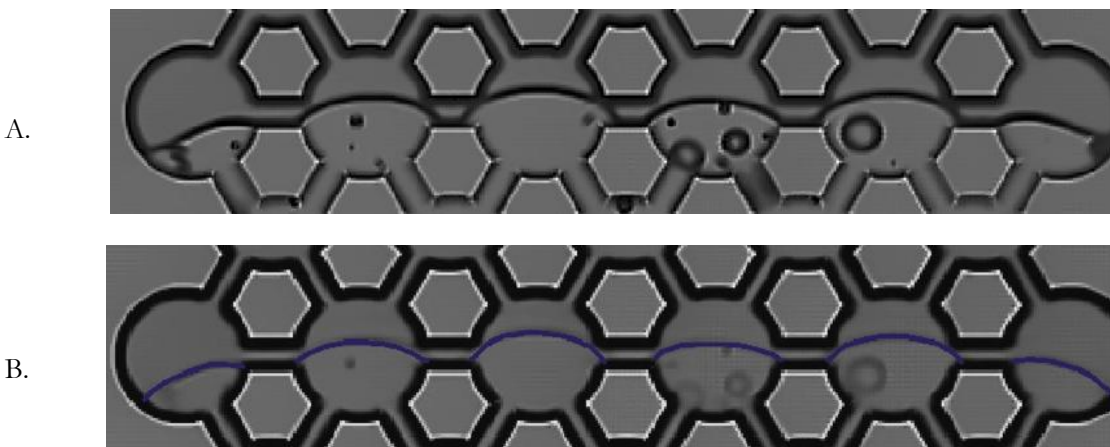


Figure 4-7. The interface during an experiment with an injection flowrate of 320 nl/min (A). In Avizo the interfacial area is coloured and measured (B).

Total fluid-fluid interfacial area is measured by using Avizo. A line is drawn along the entire interface. The interfacial area is found by counting the outer area of the line and dividing it by two.

#### 4.4.4 Wettability

Micromodels with two wetting states are under investigation. Experiments on the water-wet model will be conducted for all flowrates. To determine influence of wettability on interfacial velocity, experiments are conducted on an intermediate-wet model with an injection rate of 100 nl/min.

Wettability is measured by the contact angle. Contact angle can be determined using a single picture in which water, glass and air meet, just as in Figure 3-3 A and B. Important is that the three phase contact point is not located at a corner. As explained in Section 3.2, roughness of a surface at a corner can influence the contact angle. In Figure 4-8 two screenshots are shown to illustrate how the contact angle is determined for a water-wet micromodel (A) and an intermediate-wet model (B).

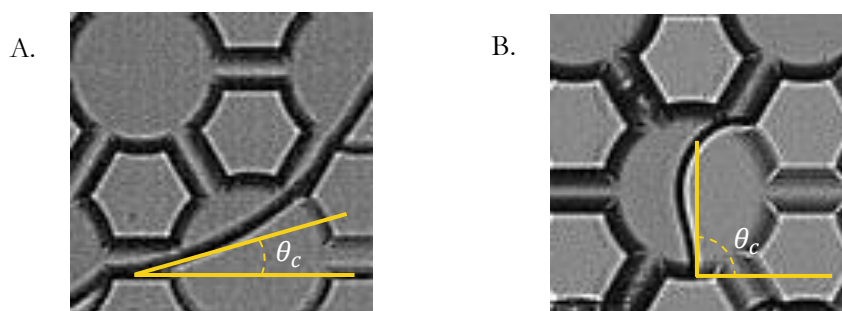


**Figure 4-8.** An example of how the contact angle is measured. **A.** shows a water-wet model, **B.** shows a intermediate-wet model.

The influence of wettability on the interfacial velocity is determined by comparison between two interfacial velocity values. In the previous Section is explained how the velocity is found.

As explained, the original wetting state of a glass micromodel is water-wet. Initially, the influence of connate water saturation on the interfacial velocities in the micromodel would be investigated. Connate water means that before waterflooding, a small amount of water is present in a porous rock. In order to establish this condition the model has to be “pre-wetted”. During this procedure the wettability of the micromodel has changed unintentionally. In the model humid air of about 40 °C was injected. Probably along with the water another hydrophobic chemical compound deposited on the glass surface, making it more oil wet. The models are now used to investigate the influence of wettability on the meniscus dynamics. In this report the influence of connate water saturation is not investigated.

## 5 Measurements and calculations

In this Chapter the measurements and calculations are presented. In the sequential Chapter the findings and conclusions will be discussed. Lastly, final conclusions and major findings are presented in Chapter 7. Results, like interfacial velocity and event flowrate, are always based on the average of five similar events.

### 5.1 Types of events

Water-air displacement is captured on camera and the images have been analyzed. During displacement air filled pores are invaded by water. When the interface moves across a pore-body, it will separate as soon as it reaches the top of the pore-body. The separation of the interface is called a “pore-filling event” or “event” in short.

When the results were first examined, it became clear that three different types of events could be distinguished, based on the geometry of interface splitting. Reason they were divided in categories is because the behaviour was not known. And therefore it could be that certain events behave in a different way. Later on, it appeared that event type is of no significant influence on the behaviour.

The geometry determines the name of the event, e.g. the name C-event is derived from the way air filled pore-necks are connected for this type of event: they form a “C” shape in the initial situation. The next three Sections will explain the course of the events using animations. The actual images can be found in Appendix B.

#### 5.1.1 C-events

In Figure 5-1 a schematic representation of a C-event is shown. As water (displayed red) is injected, air (displayed gray) is pushed out of the pore-body (1). Due to surface tension the interface behaves as a stretched membrane and doesn't want to be separated. Eventually the interface is pushed towards the sharp corner (2). After separation of the interface, water invades the two necks (3).

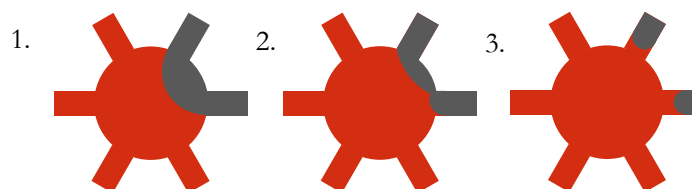


**Figure 5-1. A schematic representation of a C-event. The wetting phase is displayed red and the non-wetting phase gray. Flow is coming from bottom up and pushing the interface toward a sharp corner, where it is separated.**

#### 5.1.2 E-events

Figure 5-2 shows schematically how a typical E-event progresses. This type of event occurs in three pore-necks (1). When water invades the pore-body, one of the outer necks gets partially invaded. In this way the interface is able to move towards a corner (2), where it eventually splits (3).

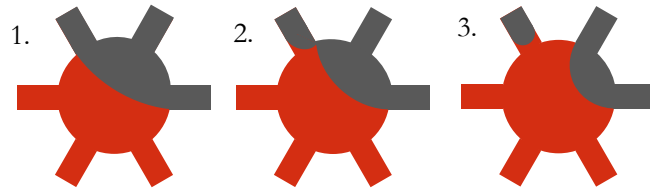


Figure 5-2. A schematic representation of an E-event. The wetting phase is displayed red and the non-wetting phase gray. Flow is coming from bottom down and pushing the interface toward a sharp corner, where it is separated.

### 5.1.3 W-events

A typical W-event is displayed in Figure 5-3. At first, water is present in two separated pore-bodies (1). As injection continues water penetrates the connecting pore-neck from both sides. The interface detaches from the middle pore-neck (2), which leads to separation of the interface (3).

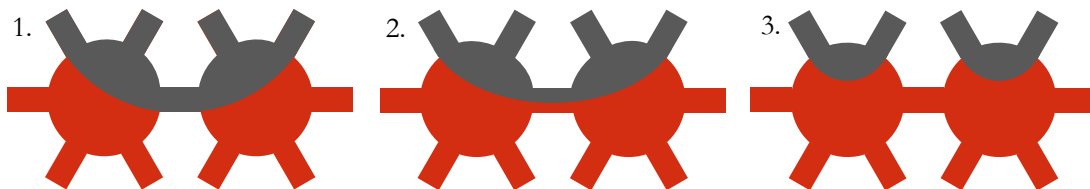
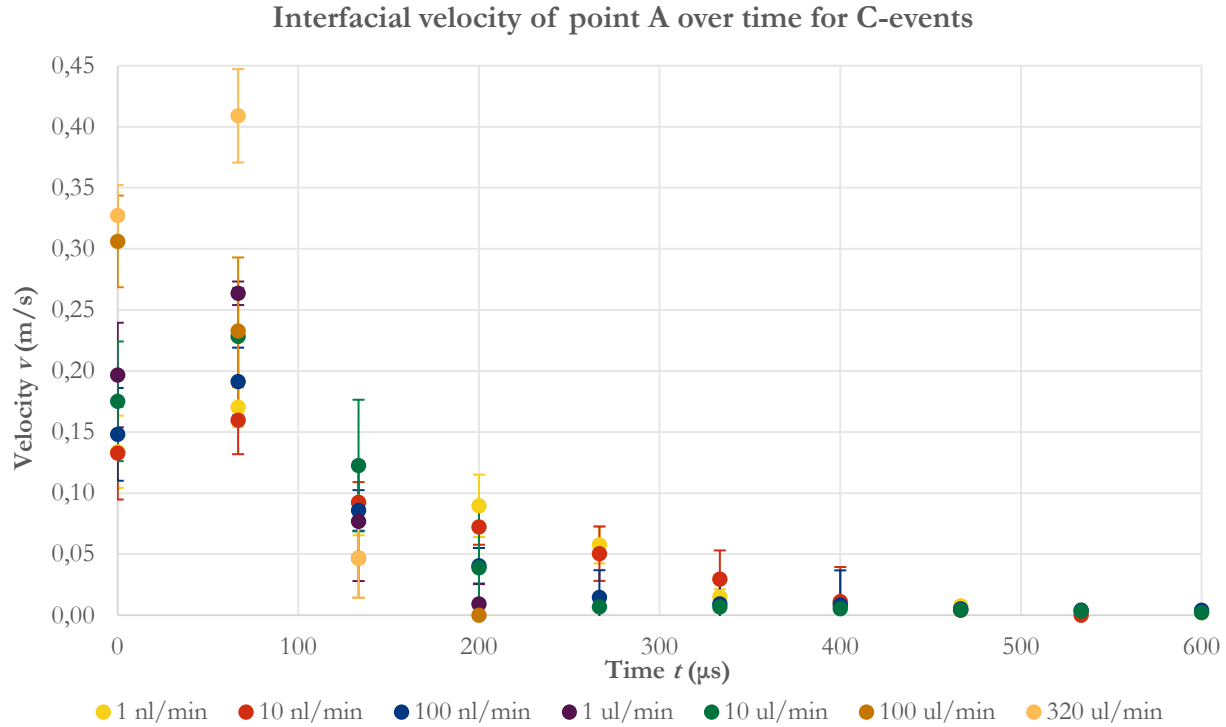


Figure 5-3. A schematic representation of a W-event. The wetting phase is displayed red and the non-wetting phase gray. Flow is coming from bottom down and pushing the interface toward a sharp corner, where it is separated.

## 5.2 Interfacial velocity

The first point of investigation is the interfacial velocity. Experiments are performed as described in Section 4.4.1 Interfacial velocity. Results of measurements on interfacial velocities are presented in Figure 5-4, where the interfacial velocity of point A is plotted for C-events over time for all flowrates.

In Section 6.2 Interfacial velocity the interfacial velocity will be compared with the front velocity.



**Figure 5-4. The velocity of point A over time for a C-event measured at three different flowrates.**

Velocity of point B was tracked as well. Also, velocities of E- and W-events were evaluated to provide a more solid base for conclusions. These can be found in Appendix C. Conclusions based on this data will be drawn in Section 6.2.

Table 5-1 gives an overview of the peak interfacial velocity, measured for each given bulk flowrate and each event type. Some places in the table are blank, because not all events occur at all flowrates. Error in the measurement is defined using the function CONFIDENCE in Excel. In this case it means that there is a 97% chance that a measurement is within the range of (AVERAGE  $\pm$  CONFIDENCE)[28]. All errors in this report are defined by the CONFIDENCE function.

**Table 5-1. Peak in interfacial velocity for all injection flowrates.**

Injection rate		$1,0 \cdot 10^0$	$1,0 \cdot 10^1$	$1,0 \cdot 10^2$	$1,0 \cdot 10^3$	$1,0 \cdot 10^4$	$1,0 \cdot 10^5$	$3,2 \cdot 10^5$
$Q_{injection}$ (nl/min)								
Displacement front velocity $v_{front}$ (m/s)		$6,7 \cdot 10^{-6}$	$6,7 \cdot 10^{-5}$	$6,7 \cdot 10^{-4}$	$6,7 \cdot 10^{-3}$	$6,7 \cdot 10^{-2}$	$6,7 \cdot 10^{-1}$	2,1
Peak in interfacial velocity $v_{peak}$ (m/s)	C-event A	$0,17 \pm 0,02$	$0,16 \pm 0,02$	$0,19 \pm 0,03$	$0,26 \pm 0,01$	$0,23 \pm 0,04$	$0,31 \pm 0,04$	$0,41 \pm 0,04$
	C-event B	$0,14 \pm 0,03$	$0,12 \pm 0,02$	$0,11 \pm 0,02$	$0,19 \pm 0,05$	$0,16 \pm 0,03$	$0,30 \pm 0,03$	$0,41 \pm 0,05$
	E-event A	$0,12 \pm 0,04$	$0,10 \pm 0,02$	$0,14 \pm 0,01$	$0,14 \pm 0,01$	$0,15 \pm 0,01$	-	-
	E-event B	$0,15 \pm 0,02$	$0,14 \pm 0,01$	$0,16 \pm 0,01$	$0,17 \pm 0,02$	$0,17 \pm 0,02$	-	-
	W-event A	-	$0,15 \pm 0,01$	$0,20 \pm 0,06$	$0,19 \pm 0,06$	-	-	-
	W-event B	-	$0,12 \pm 0,02$	$0,14 \pm 0,03$	$0,15 \pm 0,03$	-	-	-

### 5.3 Event flowrate

The main question of this report is if interfacial velocities depend on bulk flowrate. Interfacial velocities as function of time for an event are plotted for different flowrates. The interfacial dynamics dictate the velocity signature, but also the amount of air that is displaced by water. Therefore the second point of investigation is the so called event flowrate, which gives the rate at which a pore-filling event displaces the non-wetting phase during dynamic imbibition.

Figure 5-5 displays the graph of the injection flowrate as function of the event flowrate. Not all event types occur at all flowrates, and therefore not all series cover up the entire range of injection flowrates. Because the injection flowrate is increased with a factor of ten each step, the axis is plotted along a logarithmic scale with a base of 10.

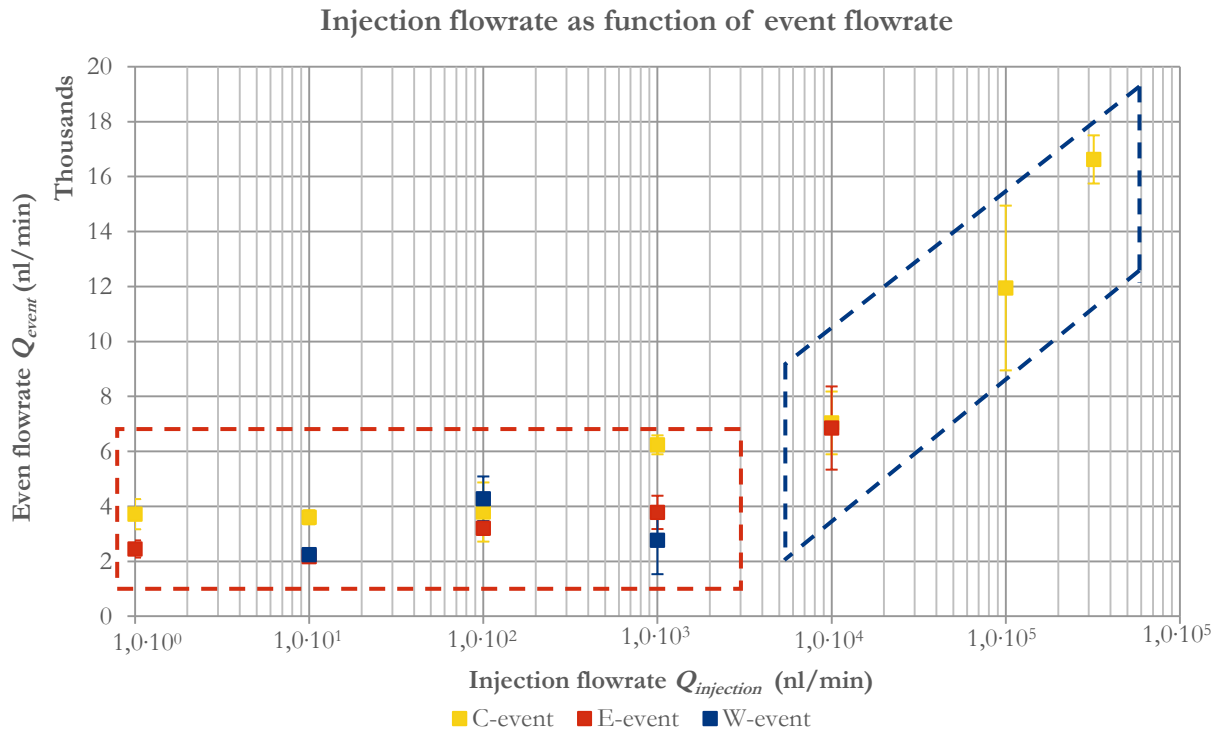


**Figure 5-5.** The event flowrate as a function of the injection flowrate. Injection flowrate is plotted on a logarithmic scale. The red box indicates the injection flowrates at which no dependence is found of the event flowrate on the injection flowrate. In the blue box the event flowrate increase with injection flowrate.

Figure 5-5 displays that for bulk flowrates from 1 nl/min to 1  $\mu$ l/min there is no increase of event flowrate when the injection rate is increased (red dashed area in Figure 5-5). That could indicate a capillary dominated system for these bulk flowrates. In the blue dashed area there seems to be a relation between injection flowrate and event flowrate. The average value of the event flowrate is for the red dashed area is obtained from Table 5-2. Further implications of this data will be given in the Section 6.3.

Table 5-2. Average event flowrate for bulk flowrates from 1 nl/min to 1  $\mu$ l/min.

Injection flowrate $Q_{injection}$ (nl/min)	$1,0 \cdot 10^0$	$1,0 \cdot 10^1$	$1,0 \cdot 10^2$	$1,0 \cdot 10^3$	Average event flowrate $Q_{event}$ (nl/min)
Displacement front velocity $v_{front}$ (m/s)	$6,7 \cdot 10^{-6}$	$6,7 \cdot 10^{-5}$	$6,7 \cdot 10^{-4}$	$6,7 \cdot 10^{-3}$	
Event flowrate for C-events $Q_{C-event}$ (nl/min)	$3,72 \cdot 10^3$	$3,60 \cdot 10^3$	$3,79 \cdot 10^3$	$6,24 \cdot 10^3$	$(3,5 \pm 0,8) \cdot 10^3$
Event flowrates for E-events $Q_{E-event}$ (nl/min)	$2,45 \cdot 10^3$	$2,17 \cdot 10^3$	$3,20 \cdot 10^3$	$3,78 \cdot 10^3$	
Event flowrate for W-events $Q_{W-event}$ (nl/min)	-	$2,24 \cdot 10^3$	$4,28 \cdot 10^3$	$2,77 \cdot 10^3$	

### 5.4 Interfacial area

The interfacial area is determined as explained in Section 4.4.3 and plotted as a function of the injection flowrate in Figure 5-6. The flowrate is plotted on a logarithmic scale with a base of ten. As one would expect, a higher flowrate results in a lower interfacial area since the displacement front is getting more stable. Remarkable is that the lowest interfacial area is found at the lowest injection rate. More explanation about this observation will be provided in section 6.4.

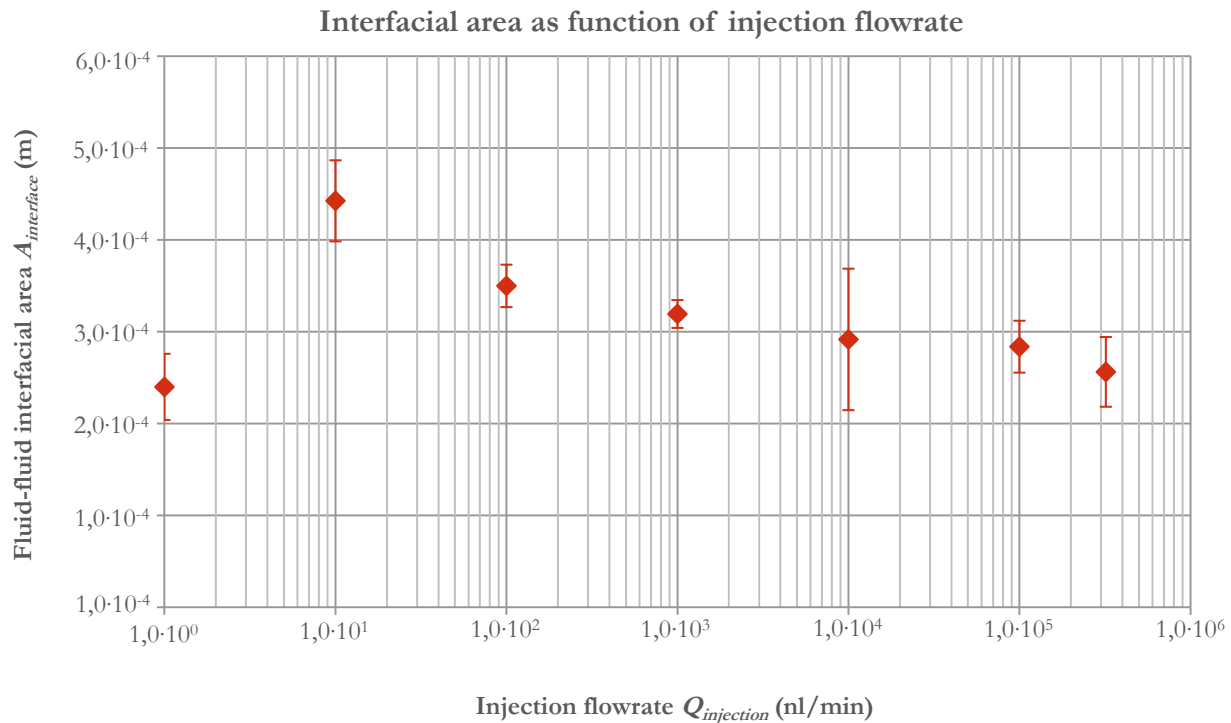


Figure 5-6. The fluid-fluid interfacial area as function of the injection flowrate.

## 5.5 Wettability

Two different wetting states of the micromodel were tested, one water-wet and one intermediate-wet model. To define the wetting state, the contact angle is determined. Results are shown in Table 5-3.

Table 5-3. Difference between the original and changed wetting conditions of the model, measured in ImageJ.

Measure point (-)	Measured contact angle water-wet micromodel $\theta_{c,ww}$ (-) $\Delta\theta_{c,ww} = \pm 0,005$	Measured contact angle intermediate-wet micromodel $\theta_{c,iw}$ (-) $\Delta\theta_{c,iw} = \pm 0,005$
1	18,4	91,4
2	19,2	90,0
2	20,1	91,6
4	17,2	89,8
5	18,0	88,9
Average	19	90
Confidence	3	4

On the intermediate-wet model the same experiments as on the water-wet model are performed, but with only a flowrate of 100 nl/min. Figure 5-7 displays the result of the interfacial velocity during C-events for both wetting situations. The same graph is made for an E-event and is displayed in Appendix D. No W-events were experienced during imbibition on the intermediate-wet model at a flowrate of 100 nl/min.

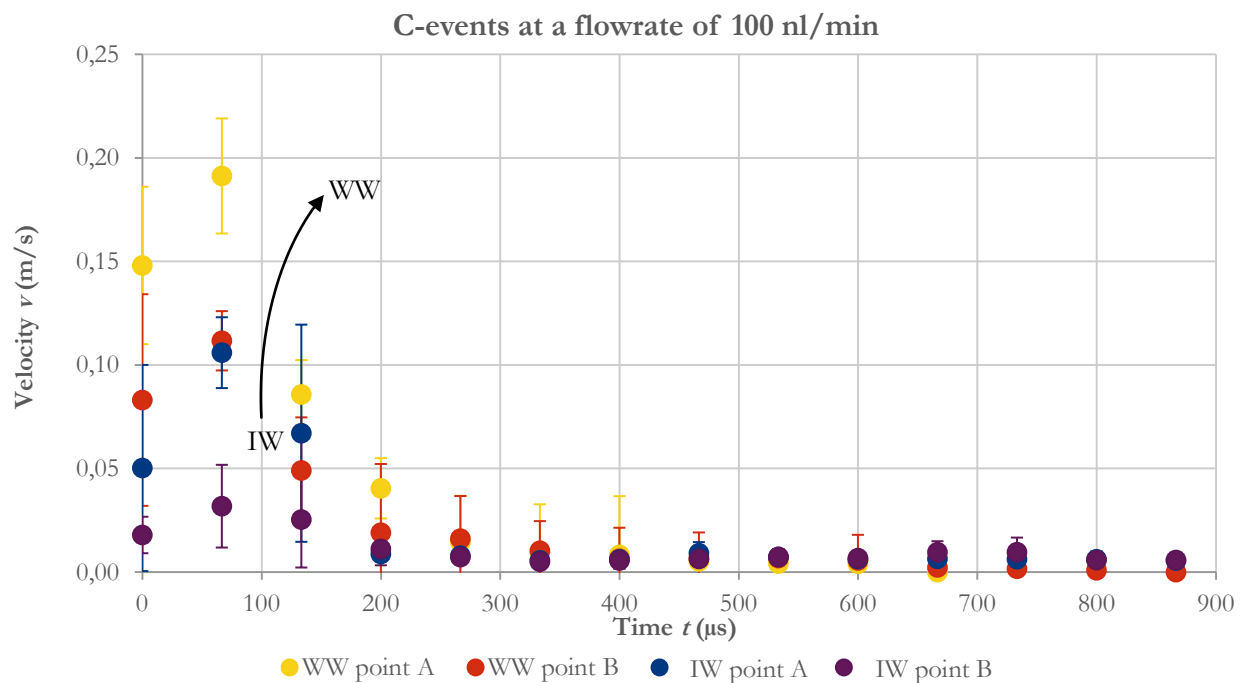


Figure 5-7. Velocity of C-events over time for the water-wet (WW) and intermediate-wet (IW) micromodels. Both point A and B are tracked. The trend in this graph is indicated by the black arrow: if wettability goes from intermediate-wet to water-wet (i.e. contact angle decreases), the interfacial velocity increases.

## 6 Results and discussions

This Chapter provides a discussion based on the results from Chapter 5. Specific research questions, as outlined in Chapter 1, will be addressed in Chapter 7.

### 6.1 Event hierarchy

In Section 5.1 the event types were categorized and in this section, an overview of the hierarchy of the events is made. The result is displayed in Figure 6-1 and shows how the events are related to each other. The term “variable” in the figure is used when no pre-determined event occurs afterwards. For example, in a C-event the interface approaches a corner and splits. Both interfaces A and B advance into a single pore-neck where it eventually enters a pore-body. Therefore, there is no way to determine what kind of sequential event will occur.

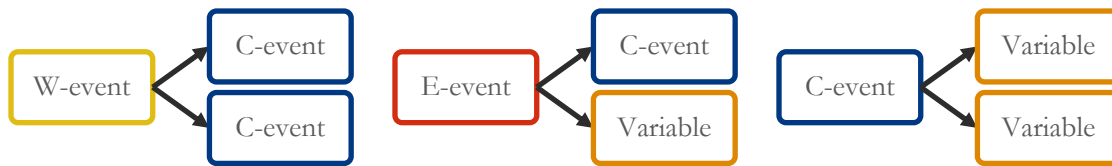


**Figure 6-1.** A diagram of the hierarchy of events. A W-event results in two C-events (left). An E-event results in a C-event and a loose variable event, and a C-event results in two variable events (right).

Additionally, not all events occur at every tested flowrate. Table 6-1 gives an overview. As displayed, W-events only occur at a flowrate of 10 nl/min, 100 nl/min or 1  $\mu$ l/min. Also, no E-events were observed at injection flowrates higher than 100  $\mu$ l/min. Explanation for this can be found by considering the conservation of mass. When injection flowrate increases, more pore bodies are filled per time unit (assuming water does not compress during injection), resulting in more events per time unit. This can indicate that W-events are a consequence of two interfering events. Combining two mirrored E-events results (geometrically speaking) into a W-event. The same also applies to E-events, they could be the consequence of two interfering C-vents. Also, the displacement front can provide an explanation. This will be discussed in Section 6.6.

**Table 6-1.** Overview of the events and the flowrate at which they occur.

Flowrate $Q_{injection}$	1 nl/min	10 nl/min	100 nl/min	1 $\mu$ l/min	10 $\mu$ l/min	100 $\mu$ l/min	320 $\mu$ l/min
Displacement front velocity $v_{front}$ (m/s)	$6,7 \cdot 10^{-6}$	$6,7 \cdot 10^{-5}$	$6,7 \cdot 10^{-4}$	$6,7 \cdot 10^{-3}$	$6,7 \cdot 10^{-2}$	$6,7 \cdot 10^{-1}$	2,1
C-event	×	×	×	×	×	×	×
E-event	×	×	×	×	×		
W-event		×	×	×			

## 6.2 Interfacial velocity

In Figure 5-4 interfacial velocities at flowrates from 1 nl/min up to 10  $\mu\text{l}/\text{min}$  overlap within the uncertainty of the measurement. Thus, the interfacial velocities are independent of the injection flowrates for these specific injection flowrates. The same conclusion can be drawn from Figure 6-2, which is the plot of data of Table 5-1. One can see that the peak velocity is constant for flowrates up to 10  $\mu\text{l}/\text{min}$ . From the velocity independence, it can be concluded that the capillary force is dominant. Viscous forces, induced by the injection of water, do not play a dominant role in displacement. This all is in good agreement with the theory of Lenormand [24] about the capillary fingering regime.

At the flowrates of 100  $\mu\text{l}/\text{min}$  and 320  $\mu\text{l}/\text{min}$  injection the interfacial velocity is significantly higher than at the lower flowrates in both figures. This indicates that viscous forces start to play a role in displacement. Probably this is within the transition or stable displacement regime, as indicated in Figure 3-10. Maximum values of interfacial velocities for all types of events and all different flowrates are displayed in Figure 6-2. In Appendix C more graphs like in Figure 5-4, only for other events, are presented.

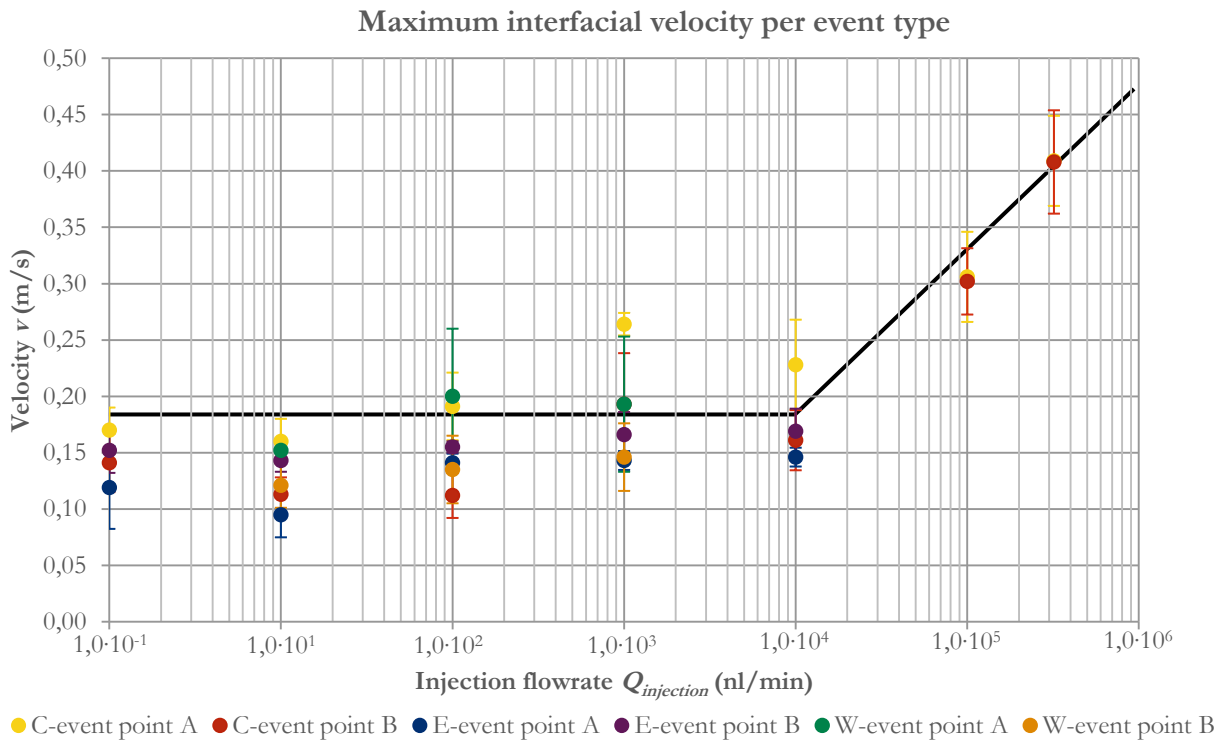


**Figure 6-2. The maximum interfacial velocity per flowrate and per event type. The black line illustrates the trend that is observed. Viscous forces start to play a role in displacement the black line starts to rise.**

Table 6-2 provides a comparison between the front velocity and the maximum interfacial velocities for three cases of injection flowrate. Difference between front velocity and interfacial velocity covers up to five orders of magnitudes. The fact that interfacial velocities exceed the front velocity in such a degree indicates that these displacements are capillary dominated and not viscous dominated.

To investigate the interfacial further, the ratio  $R_{velocity}$  is introduced.  $R_{velocity}$  gives the ratio between the interfacial velocity and the front velocity, and is defined as follows from equation (6-1):

$$R_{velocity} = \frac{v_{interface}}{v_{front}} \quad (6-1)$$

With this ratio it is possible to into further detail about the relation between velocity on the macroscopic scale and on the microscopic scale. The ratio is displayed in Table 6-2 for several injection flowrates.

**Table 6-2. For the different flowrates the front velocity and the maximum interfacial velocities are compared. The ratio  $R_{velocity}$  describes the ratio of interfacial velocity to front velocity.**

Pumprate $Q_{injection}$ (nl/min)	$1,0 \cdot 10^0$	$1,0 \cdot 10^4$	$1,0 \cdot 10^5$
Capillary number $Ca$ (-)	$9,2 \cdot 10^{-10}$	$9,2 \cdot 10^{-6}$	$9,2 \cdot 10^{-5}$
Front velocity $v_{front}$ (m/day)	0,577	577	5770
Front velocity $v_{front}$ (m/s)	$6,7 \cdot 10^{-6}$	$6,7 \cdot 10^{-2}$	6,7
Maximum interfacial velocity $v_{interface}$ (m/s)	~0.1-0.2	~0.15-0.25	~0.4
Ratio $v_{interface} : v_{front}$ (-)	2200	3,0	0,060

Based on Table 6-2 the graph in Figure 6-3 can be plotted.

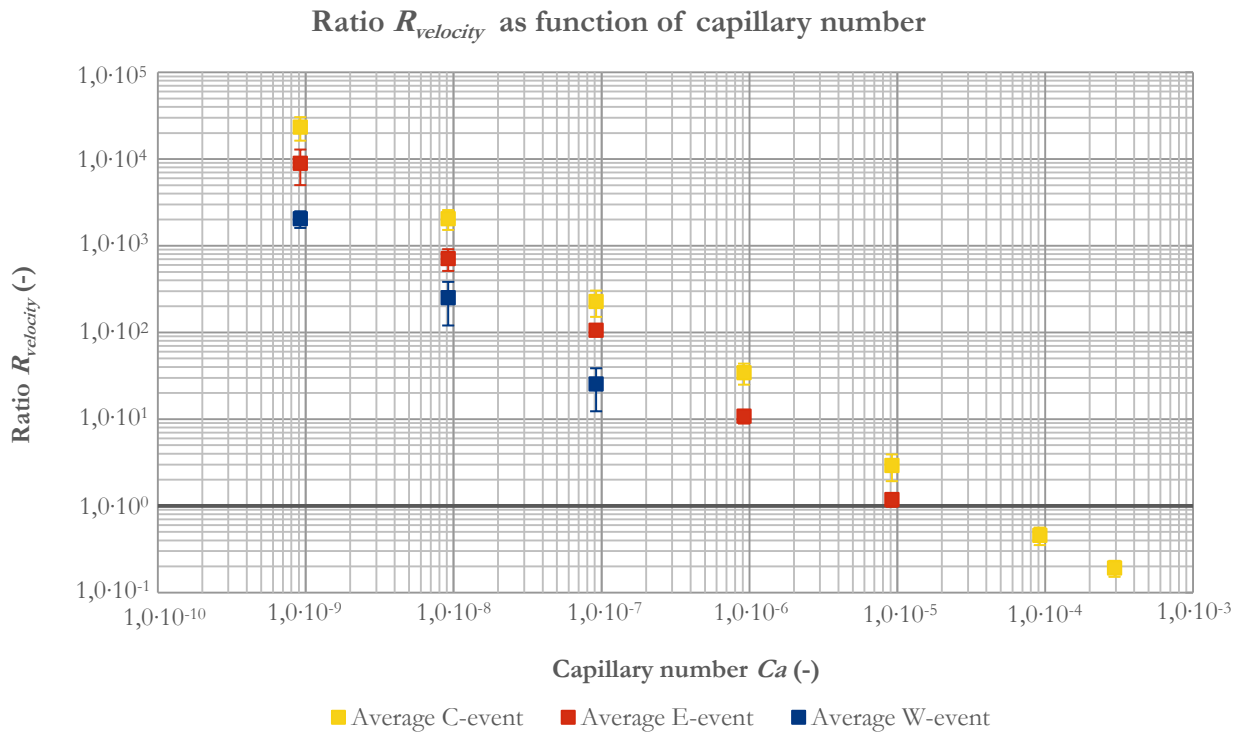


**Figure 6-3. The ratio  $R_{velocity}$  as function of the capillary number, for C-, E-, and W-events.**

From Figure 6-3 it can be obtained that low capillary numbers, corresponding with low injection flowrates, result in high ratios, i.e. that interfacial velocities are much higher than front velocities. As capillary number increases, the ratio drops linearly. At a certain point, the ration drops lower than 1, indicating that front velocity exceeds interfacial velocity.

### 6.3 Event flowrate

For all types of events and injection flowrates the event flowrate is determined. This is the rate at which a pore-filling event displaces air. The interfacial velocities do not depend on bulk flowrate for injection rates until 1  $\mu\text{l}/\text{min}$ , and therefore the event flowrate is constant as well. At higher flowrates, the event flowrate increase along with injection flowrate, as shown in Figure 6-3.

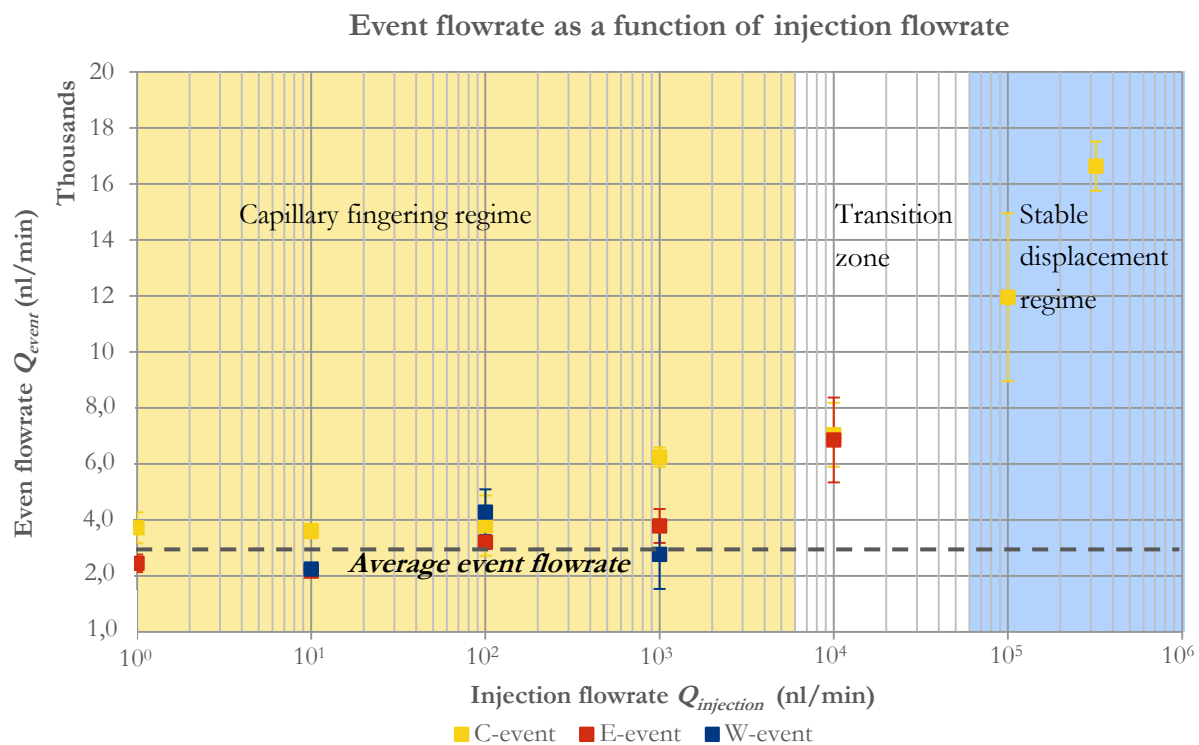


Figure 6-4. Event flowrate as a function of injection flowrate. The dashed line indicates the average event flowrate of bulk flowrates up to 1  $\mu\text{l}/\text{min}$ . Yellow marks a capillary dominated system (and thus with the capillary fingering regime), according to event flowrate measurements. Blue marks where imbibition is viscous dominated (and thus in the stable displacement regime. The transition zone is displayed in white.

The event flowrate is calculated for capillary dominated flowrates and has a value of  $(3,5 \pm 0,8) \cdot 10^3$  nl/min. As long as flow is capillary dominated, the event flowrate does not change with an increasing flowrate. Interest goes out to the point where *injection flowrate* exceeds *event flowrate*. According to the findings of Table 5-2, event flowrate is exceeded for injection flowrates from 10  $\mu\text{l}/\text{min}$  and higher. In Figure 6-3 that is the point where transition takes place, i.e. the point from which event flowrate starts to increase as injection increases. Thus,

the capillary forces dictate event flowrate as represented by the dashed line. When injection exceeds the value of the sum of all event flowrates of simultaneous events, viscous forces start to play a role in displacement.

Interest goes out to the relation between event flowrate and the injection flowrate. To investigate this relationship further, the ratio of the event flowrate to the injection flowrate is examined. This ratio is given by equation (6-2):

$$R_{flowrate} = \frac{Q_{event}}{Q_{injection}} \rightarrow Q_{event} = R \cdot Q_{injection} \quad (6-2)$$

In which:

$R_{flowrate}$	ratio of event flowrate to event flowrate	[–]
$Q_{event}$	event flowrate	[nl/min]
$Q_{injection}$	injection flowrate	[nl/min].

Ratio  $R_{flowrate}$  expresses how many times the event flowrate exceeds the injection flowrate.  $R_{flowrate}$  is calculated for all flowrates and all event types and displayed in Figure 6-4 (plotted on log-log axis), as function of injection flowrate.

When displacement is dictated by capillary forces, the interfacial velocities exceed the displacement front velocity. The same applies to the event flowrate; as long as the capillary force is dominant the event flowrate is higher than the injection flowrate. At injection of 1 nl/min the ratio  $R_{flowrate}$  is in the order of  $10^3$ . While injection increases, the ratio decreases because bulk flowrate approaches event flowrate.

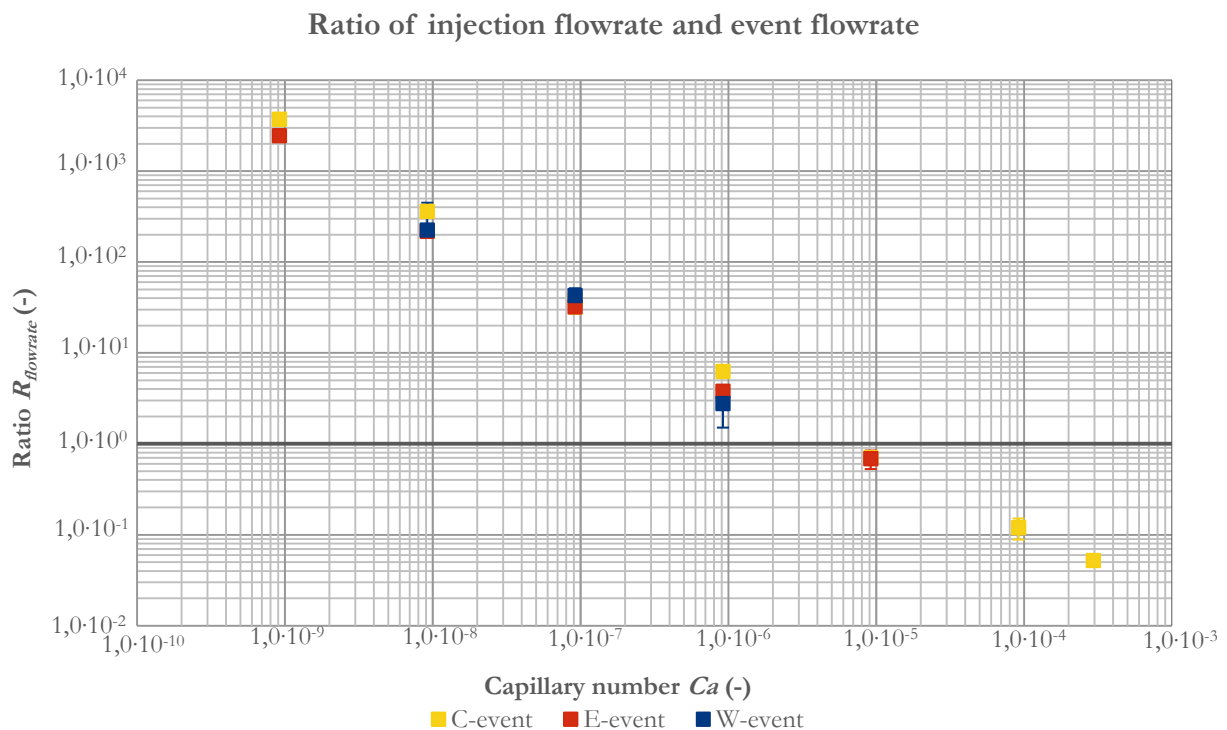


Figure 6-5. Ratio  $R$  of event flowrate to injection flowrate for all types of events as function of capillary number.

When Figure 6-5 is examined, it is clear that low capillary numbers (up to  $10^{-6}$ ) result in a ratio in the order of  $10^3$  to  $10^1$ . This indicates that the amount of air displaced during an event, is much higher than the rate at which fluid is injected. This is in good agreement with the conclusion that for these rates interfacial dynamics don not depend on injection flowrate. As the capillary number increases, the ratio drops until 0,05. This indicates that the event flowrate is lower than the injection flowrate. Since several events can occur simultaneous, this is still plausible. Also, the injection flowrate can exceed the event flowrate because not all air is displaced during events.

Figure 6-6 is considered. A displacement event takes a certain amount of time to take place, indicated with  $t_{event}$ , and sequential events take place with an interval of  $\Delta t$ . Since displacement is dominated by the intrinsic timescale, the curve of  $Q_{event}$  versus  $t$  is constant. As injection flowrate increase, more water is pumped into the system and therefore the frequency of event increases. With increasing frequency events follow much quicker and eventually overlap. That happens when the ratio  $R_{flowrate} > 1$ .

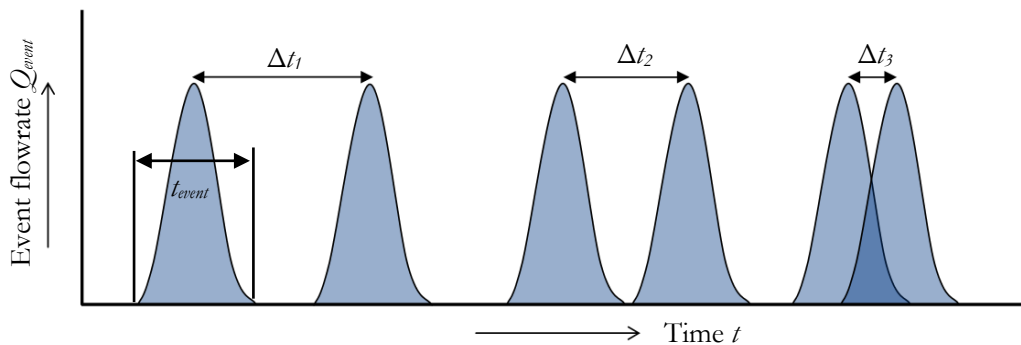
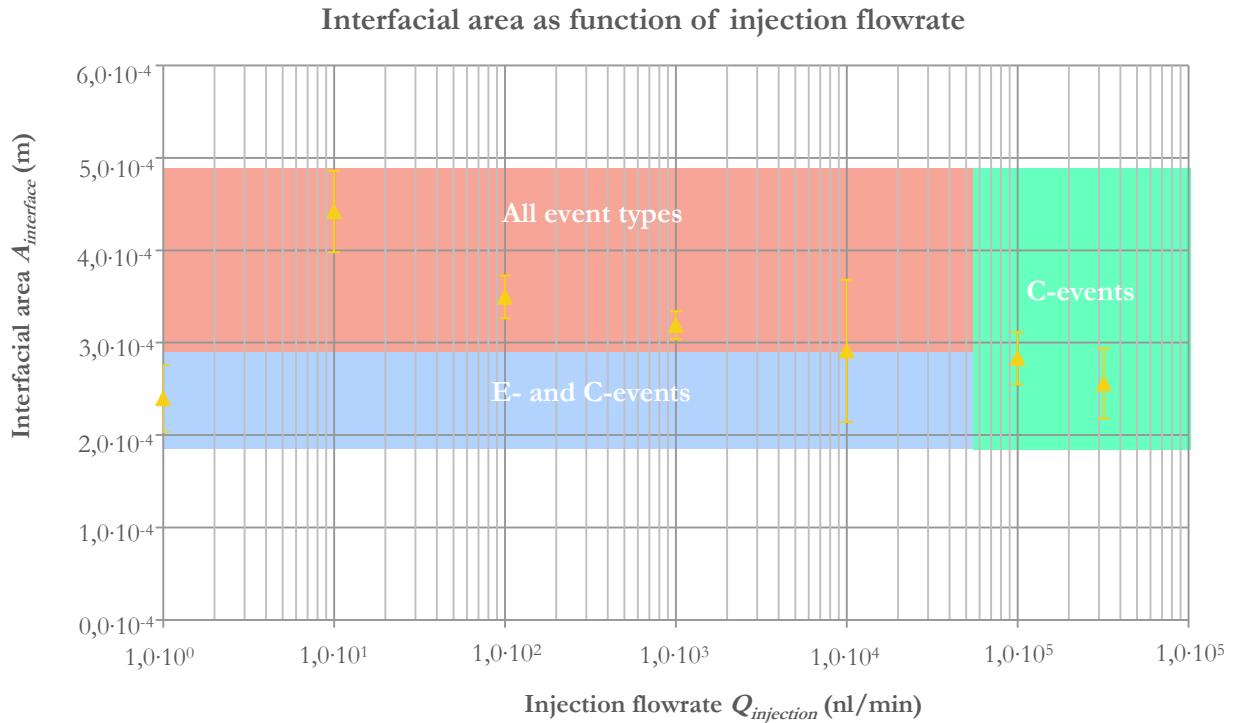


Figure 6-6. A graph illustrating the progress over time for the event flowrate.

Note that this figure is just an illustration, so no timescale or numeric value of the event flowrate can be given.

## 6.4 Interfacial area

Interfacial velocity is a parameter of single pore-scale dynamics. Interaction between behaviour on the single pore-scale and the macroscopic scale can potentially be linked by considering parameters such as interfacial area. Interfacial area (i.e. of the fluid-fluid interface) is plotted as a function of bulk flowrate in Figure 6-6. The coloured areas indicate which event types occur at the given flowrate.



**Figure 6-7. The fluid-fluid interfacial area as function of the injection flowrate. The marked areas indicate at which values of  $A_{interface}$  which events occur. In the green area only C-events occur, red indicates all event types, and blue stands for C- and E-events.**

Figure 6-4 seems to support the hypothesis that a minimum amount of interfacial area needed for W-events to occur. W-events only exist in the red area. As the injection flowrate increases, the interface becomes flatter and therefore no interference takes place. This is also illustrated by considering Figure 6-8 and Figure 6-9. The measure points within the blue area have about the same values as the ones in the green area while there is a difference in injection flowrate.

Expected is that a higher flowrate results in a flatter displacement front and therefore in a smaller interfacial area. This statement is true, except for the lowest flowrate of 1 nl/min. At this rate, the interfacial area is just as low as at 320  $\mu$ l/min injection. Explanation is found by looking at the location of the fluid-fluid interfaces. At 1 nl/min injection, only one pore-body is invaded at the time, and this happens at a very low rate (invaded pores per minut). Most of the menisci are at the end of a pore-neck, while at 320  $\mu$ l/min injection the menisci are mostly in the pore body. The area across a pore-neck differs from the area across a pore body, as illustrated in Figure 6-7. Because of this, interfacial area has its minimum at the lowest injection flowrate. This conclusion is also supported by Section 6.6, where the displacement front is considered.

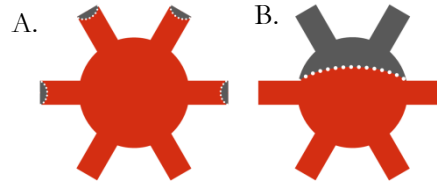


Figure 6-8. An illustration of interfacial area (white dotted lines) at lowest flowrate (A), and highest flowrate (B).

## 6.5 Wettability

As displayed in Table 5-3, two contact angles and thus two wetting states of the micromodel have been tested. While in the first case the contact angle was relatively small, indicating a water-wet system, the second case indicates an intermediate-wet situation with a large contact angle. Based on the measurements the contact angle for the water-wet situation is  $\theta_{c,ww}=(19\pm 3)^\circ$ , and for the intermediate-wet situation is  $\theta_{c,iw}=(90\pm 4)^\circ$ .

Figure 5-7 tells that there is a clear influence of the wettability on the interfacial velocities. Both point A and B follow the same profile in both water-wet and intermediate-wet situation. But, for the intermediate-wet situation the peak velocities are significantly lower. A possible explanation can be found by looking at the formula for the capillary pressure, which relates contact angle to the pressure difference across an interface. See equation (3-5).

For this experiment the same geometry was used in both water-wet and intermediate-wet models, and no change in interfacial tension was made. So *any* change in interfacial velocity has to do with the change in contact angle. With a lower capillary pressure the driving force of the motion becomes lower, resulting in a lower interfacial velocity. Since the intermediate-wet model has a contact angle of about 90 degrees, the capillary pressure almost equals 0<sup>5</sup>. This makes that the system is no longer capillary dominated, so therefore the system is viscous dominated. Because of the conservation of mass, for both water-wet and mixed-wet situation the displaced volume has to be equal. This means that with a lower interfacial velocity the distance between two simultaneous and/or sequential events must decrease.

Sometimes, capillary number is calculated as displayed in equation (6-4):

$$Ca = \frac{v_{Darcy} \cdot \mu}{\sigma \cdot \cos \theta_c} \quad (6-4)$$

When imbibition in water-wet models is examined, the contact angle is relatively small and therefore the contact angle is not included in the capillary number (since  $\cos 0^\circ=1$ ). But, when an intermediate-wet model is examined, the contact angle approaches  $90^\circ$ , resulting in capillary numbers of infinity (since  $\cos 90^\circ=0$ ). In Lenormand's graph a capillary number of infinity corresponds to the stable displacement regime, while this displacement type is not experienced. Possible explanation is found by considering the application of the equation (6-4) to the capillary number to the situation of a micromodel. The formula is less applicable when

<sup>5</sup> However, there is likely still a capillary pressure since the contact angle that is measured is an apparent angle, measured under dynamic conditions where the current equations do not apply.

more complex geometries are studied. Also, as the contact angle in a pore-neck may be  $90^\circ$ , in a pore-body this is often not the case and therefore there is still a capillary pressure in the system. Thus, even in intermediate-wet systems still capillary forces are present.

## 6.6 Macroscopic displacement front

While the interfacial area gives quantitative analyses of the macroscopic displacement front, the front is investigated by its advancement over time. Figures of the front are created by overlaying four screenshots from the imbibition videos. Injection rate varies, and therefore the time between to frames varies as well and will be mentioned in the caption. The colour of the displacement front indicates which shape the front had at a certain moment in time, the order is yellow ( $t=t_0$ ), red ( $t=t_1$ ), blue( $t=t_2$ ), purple( $t=t_3$ ). If certain parts of the front do not change from one frame to another, the colour of the previous frame remains. Figure 6-8 displays the displacement front during imbibition at a flowrate of 1 nl/min, and Figure 6-9 is made at a flowrate of 320  $\mu\text{l}/\text{min}$ . Displacement fronts at other rates can be found in Appendix E.

Figure 6-8 and Figure 6-9 show two outer cases of the injection flowrate and will illustrate the transition in displacement front. During injection at 1 nl/min only one pore-body gets filled at the time, resulting in capillary fingering. As concluded from previous Sections, displacement is capillary dominated. Although the width of the channel may limit the visual observation of this regime, the difference with the displacement front at 320  $\mu\text{l}/\text{min}$  is significant. In the latter case the front is stable. The pump rate overrules the intrinsic timescale, meaning that the frontal velocity is higher than the interfacial velocity. This supports previous conclusions from Section 6.3 and 6.4.

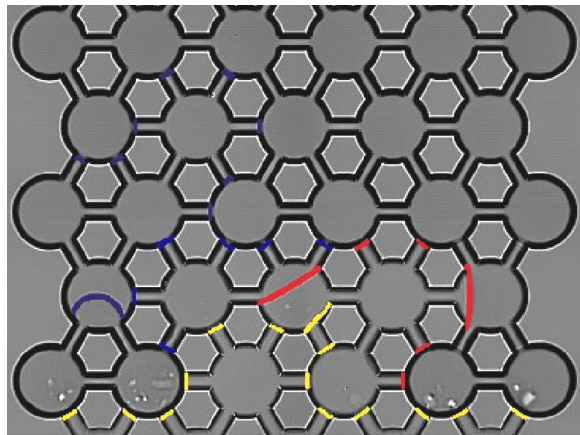
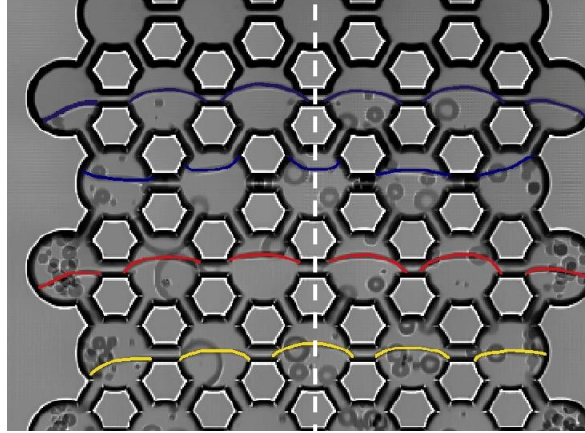


Figure 6-9. Displacement front at an injection flowrate of 1 nl/min. Four frames of the video images have been overlaid to show the progression over time. The colour of the front indicates where the interface was present at what time. The order is: yellow, red, blue, purple. Flow is coming in from bottom up and the time step between two fronts is 91 ms. This images shows displacement the capillary fingering regime.



**Figure 6-10. Displacement front at an injection flowrate of 320  $\mu\text{l}/\text{min}$ . Four frames of the video images have been overlaid to show the progression over time. The colour of the front indicates where the interface was present at what time. The order is: yellow, red, blue, purple. Flow is coming in from bottom up and the time step between two fronts is 0,24 ms. This images shows displacement the stable displacement regime.**

Figure 6-9 shows a lot of air bubbles travelling along with the displacement front. This is caused by the mobilization of trapped non-wetting phase. This only occurs at high values of the capillary number.

Another observation based on these figures concerns symmetry in a single front. At low flowrates the front is irregular (see Figure 6-8), as typically found in the capillary fingering regime (see Figure 3-10). As the flowrate increase the front becomes flatter, i.e. the font is only present in one row of pore-bodies. At flowrates of 100  $\mu\text{l}/\text{min}$  and up the front becomes perfectly symmetrical, meaning that one single front can be mirrored across the white dashed line in Figure 6-9, which is characteristic for stable displacement. Since the shape of the porous pattern is repetitive, the shape of the interface is repetitive as well at these flowrates. When two interfaces are compared in similar (but not the same) geometrical situations, their appearance is identical. From this fact it is concluded that the injection flowrate (viscous force) has overcome local imperfections in the micromodel fabrication and that displacement is viscous dominated.

The water-wet micromodel has a relatively small contact angle. During injection at low flowrates the meniscus has a shape as displayed in Figure 6-10 A. It is clear that water tends to wet the glass surface. As injection increases, the interface changes shape as displayed in Figure 6-10 B. In this case it seems like the system has change from water-wet to oil-wet. This cannot be the case because the wetting state is still the same. Reason for this phenomenon is unknown. An explanation could be that water injection occurs so fast that pressure starts to build up, in such degree that pressure of the wetting phase exceeds pressure of the non-wetting phase resulting in a “reversed” meniscus. Another reason could be that contact point pinning at corners has a large yield stress that must be overcome.

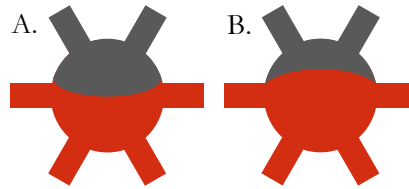


Figure 6-11. A meniscus in a single pore during imbibition experiments at low flowrates (up to 10  $\mu\text{l}/\text{min}$ ) (A.) and at high flowrates (from 100  $\mu\text{l}/\text{min}$  and up) (B.). Even though wetting conditions in both pores are the same, the meniscus has reversed, indicating that pressure in the wetting phase is higher than pressure in the non-wetting phase.

More images on the displacement front can be found in Appendix E. Based on the observations of the figures in Appendix E, boundaries of Lenormand's graph as displayed in Figure 3-10 can be readjusted. Such, that they represent the glass micromodel in this study. The result is shown in Figure 7-1.

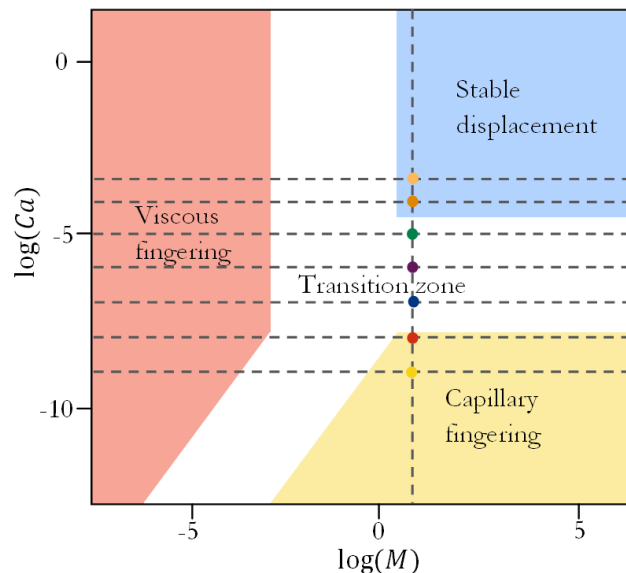


Figure 7-1. A schematic representation of the displacement regimes. Boundaries of the regimes are based on observations and conclusions of this study. Injection flowrate was varied from 1  $\text{nl}/\text{min}$  (yellow) to 320  $\mu\text{l}/\text{min}$  (light brown).

Note that only the  $y$ -axis is adjusted, because no measurements are performed with other values for the mobility ratio. Also, nothing can be pronounced about the location of viscous fingering regime, because this regime was not observed during one of the measurements. The figure is made by visual observations of the displacement front. The figure would be different if the interfacial velocity or event flowrate is considered.



## 7 Conclusions

Interfacial velocities during dynamic imbibition were studied in two-dimensional glass micromodels. Dynamic imbibition was carried out with water as wetting phase and air as non-wetting phase. Objectives for this project are described below, together with their conclusions.

I. *Produce pore-scale video images of pore-scale mechanisms during imbibition with a high speed camera.*

Video images have been recorded successfully of dynamic imbibition in a water-wet micromodel. Screenshots can be found in Figure 4-4 and also in Appendix B. Based on their geometry, three types of events were distinguished: C-, E-, and W-events.

II. *Measure interfacial velocities at different flowrate.*

Interfacial velocities have been measured. Absolute peak values of interfacial velocity as function of injection flowrate is evaluated.

III. *Evaluate if interfacial velocities are flowrate dependent.*

Interfacial velocity is determined for bulk flowrates of 1 nl/min to 320  $\mu\text{l}/\text{min}$  (capillary numbers of  $9,2 \cdot 10^{-10}$  to  $2,9 \cdot 10^{-4}$ ) with steps of one order of magnitude. From this the following is concluded:

- (a) interfacial velocities are independent on injection flowrate, for flowrates lower than 10  $\mu\text{l}/\text{min}$ , and that
- (b) interfacial velocities depend on injection flowrate, for flowrates of 100  $\mu\text{l}/\text{min}$  and 320  $\mu\text{l}/\text{min}$ .

This conclusion is based on interfacial velocities measurements, event flowrate measurements and displacement front measurements. Interfacial velocities and event flowrates at the lower flowrates overlap within the uncertainty. This indicates that interfacial velocities are independent of the bulk flowrate.

IV. *Investigate the influence of the contact angle on the interfacial dynamics of the system.*

Measurements were conducted on micromodels with two wetting states: water-wet (contact angle  $\theta_{c,ww}=(19 \pm 3)^\circ$ ) and intermediate-wet (contact angle  $\theta_{c,iw}=(90 \pm 4)^\circ$ ). On the water-wet model all flowrates as described above are performed. On the intermediate wet model, experiments have been conducted at an injection flowrate of 100 nl/min.

Interfacial velocities were plotted for a flowrate of 100 nl/min for both models. It is concluded that velocity in the IW model are significantly lower than for the WW model. A possible explanation is found by considering capillary pressure. When the contact angle approaches  $90^\circ$  the capillary pressure goes to zero. This results in a viscous dominated system, and therefore interfacial velocities of an IW system are lower than in a WW system.



## 8 Future work

For future work, it would be interesting to validate this project by performing dynamic imbibition experiments, but with oil as non-wetting fluid and water as wetting fluid. Oil will be represented by decane. This was not done initially because of the intensive cleaning procedure when using oil. Also, the result is less repeatable because the models have to be flushed three times: first water, then decane, then water (imbibition). Furthermore, decane can also influence wettability of the system which is unwanted.

In practice, water often contains a surfactant (to reduce interfacial tension), salt, or a polymer solution (to increase water's viscosity and reduce viscous fingering in heavy oils). The presence of these compounds influence the interfacial behaviour during waterflooding. Therefore, it would be interesting to take these into account by performing the same experiments and evaluate the behaviour when either a surfactant, salt or a polymer is used. Measurements will help to explore other trajectories on the Lenormand graph (see Figure 3-10).

Currently, much effort has been put in establishing pre-wetting conditions in the micromodel. One attempt did result in the aimed pre-wetting situation, but also the wettability had changed. Now, attempts are done with glass syringes instead of plastic ones. Unfortunately there are difficulties, because the entry pressure of the model cannot be overcome by a glass syringe. Right now, attempts are still carried out to find ways to create little water saturation in the model. The aim is to perform experiments to investigate flowrate dependency of interfacial dynamics.



## 9 Acknowledgments

First of all many thanks go out to Ryan Armstrong, my daily supervisor for this project. He helped me from the very start to the end. Along the way he never hesitated to view results together and discuss on them. Also, Ryan is a good teacher and very patient, which makes it very pleasant to work with him. Other colleagues also helped on discussing the results, including Steffen Berg and Axel Makurat. Many thanks go out to them as well.

Also Rob Neiteler is acknowledged for the design of the micromodel holder and Katie Humphry is acknowledged for the design of the micromodel pattern.

Two Open Source Physics computer programs are used, which made it possible to process the data. Both ImageJ and Tracker have been of great importance. Development was made possible by the National Science Foundation Grants No. DUE-0126439 and No. DUE-0442481.

Also my supervisors of The Hague University, Mrs. Vloemans and Mr. Swarts, deserve many thanks for supervision on this project. Special thanks go out to Mr. Swarts, who helped me to get in contact with Shell to find a project. Axel Makurat is also acknowledged for making it possible to do my internship at his department: Rock and Fluid Science.

For the setup every now and then some technical adjustments had to be made. The technical lab staff was always willing to help. So many thanks go out to Niels Brussee, Sebastiaan Pieterse, Hilbert van der Linde, and Ab Coorn.

Patricia van den Bos, Pedro Zuiderwijk, Holger Ott, and Arjan van der Linden deserve acknowledgements as well. I really enjoyed working with them, even though we did not co-operate on the technical content.

Last, but certainly not least, Maaïke is acknowledged for her moral support and believe in me throughout the entire internship.

Tom van Beusekom



## 10 Bibliography

- [1] U. E. I. Administration, “INTERNATIONAL ENERGY OUTLOOK 2013,” U.S. Department of Energy, Washington, DC, 2013.
- [2] D. Koroteev, O. Dinariev, N. Evseev, D. Klemin, S. Safonov, O. Gurpinar, S. Berg, C. v. Kruijsdijk, M. Myers, L. Hathon, H. d. Jong and R. Armstrong, “Application of Digital Rock Technology for Chemical EOR Screening,” *SPE International*, 2013.
- [3] “Geology of petroleum,” Kansas Geological Survey - The University of Kansas, April 2001. [Online]. Available: <http://www.kgs.ku.edu/Publications/Oil/primer03.html>. [Accessed 1 October 2013].
- [4] “Reservoir,” Schlumberger, [Online]. Available: <http://www.glossary.oilfield.slb.com/en/Terms/r/reservoir.aspx>. [Accessed 30 September 2013].
- [5] “Caprock,” Schlumberger, [Online]. Available: <http://www.glossary.oilfield.slb.com/en/Terms/c/caprock.aspx>. [Accessed 30 September 2013].
- [6] “Primary recovery,” Schlumberger, [Online]. Available: [http://www.glossary.oilfield.slb.com/en/Terms/p/primary\\_recovery.aspx](http://www.glossary.oilfield.slb.com/en/Terms/p/primary_recovery.aspx). [Accessed 30 September 2013].
- [7] “Secondary recovery,” Schlumberger, [Online]. Available: [http://www.glossary.oilfield.slb.com/en/Terms/s/secondary\\_recovery.aspx](http://www.glossary.oilfield.slb.com/en/Terms/s/secondary_recovery.aspx). [Accessed 2013 September 2013].
- [8] I. Sandrea and R. Sandrea, “GLOBAL OIL RESERVES-1: Recovery factors leave vast target for EOR technologies,” *Oil&Gas Journal*, 11 May 2007. [Online]. Available: <http://www.ogj.com/articles/print/volume-105/issue-41/exploration-development/global-oil-reserves-1-recovery-factors-leave-vast-target-for-eor-technologies.html>. [Accessed 13 November 2013].
- [9] G. P. Willhite, *Waterflooding*, Richardson, Texas, USA: Society of Petroleum Engineers, 1986, pp. 5-52.
- [10] “Waterflooding,” Schlumberger, [Online]. Available: <http://www.glossary.oilfield.slb.com/en/Terms/w/waterflooding.aspx>. [Accessed 30 September 2013].

- [11] "Tertiary recovery," Schlumberger, [Online]. Available: [http://www.glossary.oilfield.slb.com/en/Terms/t/tertiary\\_recovery.aspx](http://www.glossary.oilfield.slb.com/en/Terms/t/tertiary_recovery.aspx). [Accessed 30 September 2013].
- [12] A. Agrawal, "Introduction to Surface Tension," Massachusetts Institute of Technology, [Online]. Available: <http://web.mit.edu/nmf/education/wettability/intro.html>. [Accessed 23 October 2013].
- [13] "Surface tension," Kibron, [Online]. Available: <http://www.kibron.com/surface-tension>. [Accessed 13 November 2013].
- [14] F. Dullien, "Surface between two fluids," in *Porous media - Fluid Transport and Pore Structure*, San Diego, California, Academic Press, Inc., 1979, pp. 118-128.
- [15] G. P. Willhite, "Effects of Reservoir Rock and Fluid Properties on the Efficiency of Linear Displacement," in *Waterflooding*, Richardson, Texas, US, Society of Petroleum Engineers, 1986, pp. 85-86.
- [16] W. Abdallah, J. S. Buckley, A. Arnegie, J. E. B. Herold, E. Fordham, A. Graue, T. Signer, H. Hussian, B. Montaron and M. Zaiuddin, "Fundamentals of Wettability," *Oilfield Review*, vol. 19, no. 2, pp. 44-61, 2007.
- [17] F. Dullien, "Equilibrium at a Line on Contact, Young's Equation," in *Porous media - Fluid Transport and Pore Structure*, San Diego, California, Academic Press, Inc., 1979, pp. 122-125.
- [18] S. Middleman, "Capillary hydrostatics: the Young-Laplace equation," in *An Introduction to Fluid Dynamics*, New York, John Wiley & Sons, Inc., 1998, pp. 39-42.
- [19] F. Dullien, "Capillary Pressure," in *Porous Media - Fluid Transport and Pore Structure*, San Diego, California, Academic Press, Inc., 1979, pp. 128-132.
- [20] G. P. Willhite, "Capillary Pressure," in *Waterflooding*, Richardson, Texas, US, Society of Petroleum Engineers, 1986, pp. 9-10.
- [21] E. W. Washburn, "The Dynamics of Capillary Flow," *Physical Review*, vol. XVIII, no. 3, pp. 273-283, 1921.
- [22] S. Middleman, "Flow Through Porous (Consolidated) Materials," in *An Introduction to Fluid Dynamics*, New York, John Wiley & Sons, Inc., 1998, p. 418.

- [23] “Capillary number,” Schlumberger, [Online]. Available: [http://www.glossary.oilfield.slb.com/en/Terms/c/capillary\\_number.aspx](http://www.glossary.oilfield.slb.com/en/Terms/c/capillary_number.aspx). [Accessed 17 December 2013].
- [24] R. Lenormand and E. Touboul, “Numerical models and experiments on immiscible displacement in porous media,” *Journal of Fluid Mechanics*, vol. 189, pp. 165-187, 1988.
- [25] “Wet etching,” Micronit microfluidics, [Online]. Available: <http://www.micronit.com/what-we-do/glass-technologies/wet-etching/>. [Accessed 29 October 2013].
- [26] “Bonding,” Micronit Microfluidics, [Online]. Available: <http://www.micronit.com/what-we-do/glass-technologies/bonding/>. [Accessed 29 October 2013].
- [27] A. Agrawal, “Wettability, non-wettability and contact angle hysteresis,” Massachusetts Institute of Technology, [Online]. Available: <http://web.mit.edu/nmf/education/wettability/wetting.html>. [Accessed 6 December 2013].
- [28] “CONFIDENCE,” Microsoft Office, [Online]. Available: <http://office.microsoft.com/en-us/excel-help/confidence-HP005209021.aspx>. [Accessed 11 December 2013].
- [29] W. Buesink, „Etch data CU585.008 project,” Micronit microfluids, Enschede, 2013.
- [30] D. C. Giancoli, “Viscositeit,” in *Natuurkunde deel 1: Mechnica en thermodynamica*, Amsterdam, Pearson Education Benelux, 2007, p. 412.
- [31] “Crude oil,” Schlumberger, [Online]. Available: [http://www.glossary.oilfield.slb.com/en/Terms/c/crude\\_oil.aspx](http://www.glossary.oilfield.slb.com/en/Terms/c/crude_oil.aspx). [Accessed 30 September 2013].
- [32] “Petroleum,” Schlumberger, [Online]. Available: <http://www.glossary.oilfield.slb.com/en/Terms/p/petroleum.aspx>. [Accessed 30 September 2013].
- [33] “What Is EOR, and How Does It Work?,” Rigzone, [Online]. Available: [http://www.rigzone.com/training/insight.asp?insight\\_id=313](http://www.rigzone.com/training/insight.asp?insight_id=313). [Accessed 30 September 2013].
- [34] A. Sheludko, “Equilibrium at the boundry of three phases. Contact angle,” in *Colloid Chemistry*, Amsterdam, Elsevier Publishing Company, 1966, pp. 90-92.
- [35] “Meniscus,” Wikipedia, 20 August 2013. [Online]. Available: <http://en.wikipedia.org/wiki/Meniscus>. [Accessed 11 September 2013].

- [36] “Cohesive and Adhesive Forces,” University of California, [Online]. Available: [http://chemwiki.ucdavis.edu/Physical\\_Chemistry/Physical\\_Properties\\_of\\_Matter/Atomic\\_and\\_Molecular\\_Properties/Intermolecular\\_Forces/Cohesive\\_And\\_Adhesive\\_Forces](http://chemwiki.ucdavis.edu/Physical_Chemistry/Physical_Properties_of_Matter/Atomic_and_Molecular_Properties/Intermolecular_Forces/Cohesive_And_Adhesive_Forces). [Accessed 23 October 2013].
- [37] R. T. Armstrong and S. Berg, “Interfacial velocities and capillary pressure gradients during Haines jumps,” *Physical Review E*, 2013.
- [38] “Porosity,” Schlumberger, [Online]. Available: <http://www.glossary.oilfield.slb.com/en/Terms/p/porosity.aspx>. [Accessed 10 December 2013].

# Appendices

## Appendix A: dimensions of glass micromodel

Table A1. The dimensions of the channels in the two glass plates, which are bonded together to form the micromodel[29].

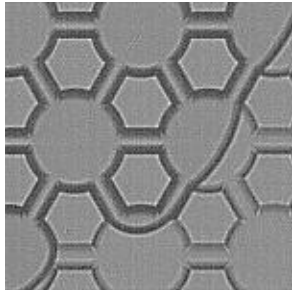
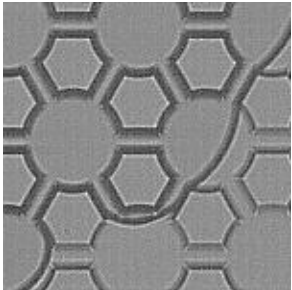
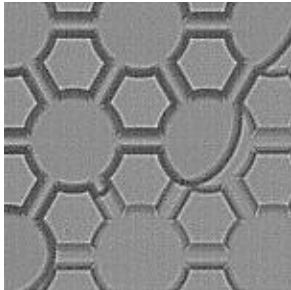
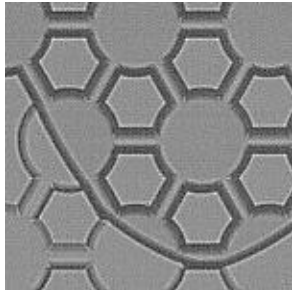
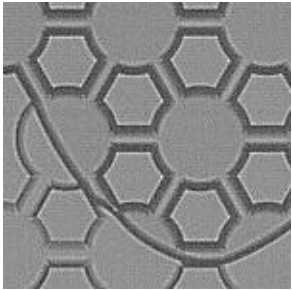
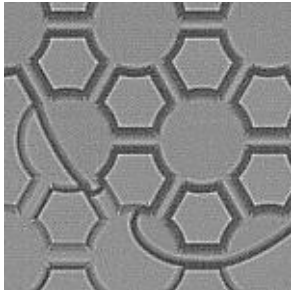
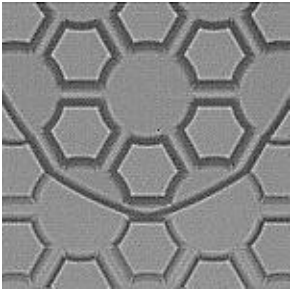
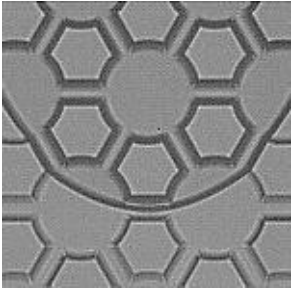
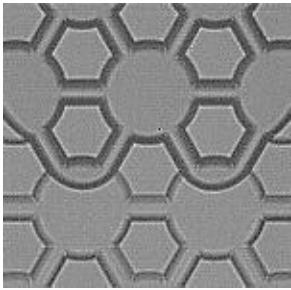
	Target depth $d_{target}$ ( $\mu\text{m}$ )	Depth measured $d$ ( $\mu\text{m}$ )			Target width $w_{target}$ ( $\mu\text{m}$ )	Width measured $w$ ( $\mu\text{m}$ )		
		Average	Max	Min		Average	Max	Min
Upper glass plate	5,00	5,06	5,01	5,15	13,00	13,01	12,80	13,61
Bottom glass plate	5,00	5,22	5,12	5,28	13,00	13,89	13,62	14,48

Table A2. Dimensions of the micromodel, based on the manufacturer's specifications [29].

Description	Dimension
Channel depth $d_{channel}$ ( $\mu\text{m}$ )	(10,3 $\pm$ 0,2)
Channel width $w_{channel}$ ( $\mu\text{m}$ )	(14 $\pm$ 1)
Pore-body diameter $D_{channel}$ ( $\mu\text{m}$ )	(60 $\pm$ 1)
Pore-neck length $l_{neck}$ ( $\mu\text{m}$ )	(20 $\pm$ 1)

## Appendix B: screenshots event types

Table B1. Typical images from the three different event types. These images are recorded at an injection flowrate of 100 nl/min.

Event type	Before interface separation $t = 0$ s	Moment of interface separation $t = 0,40 \mu\text{s}$	After interface separation $t = 0,53 \mu\text{s}$
C-event			
E-event			
W-event			

### Appendix C: interfacial velocities

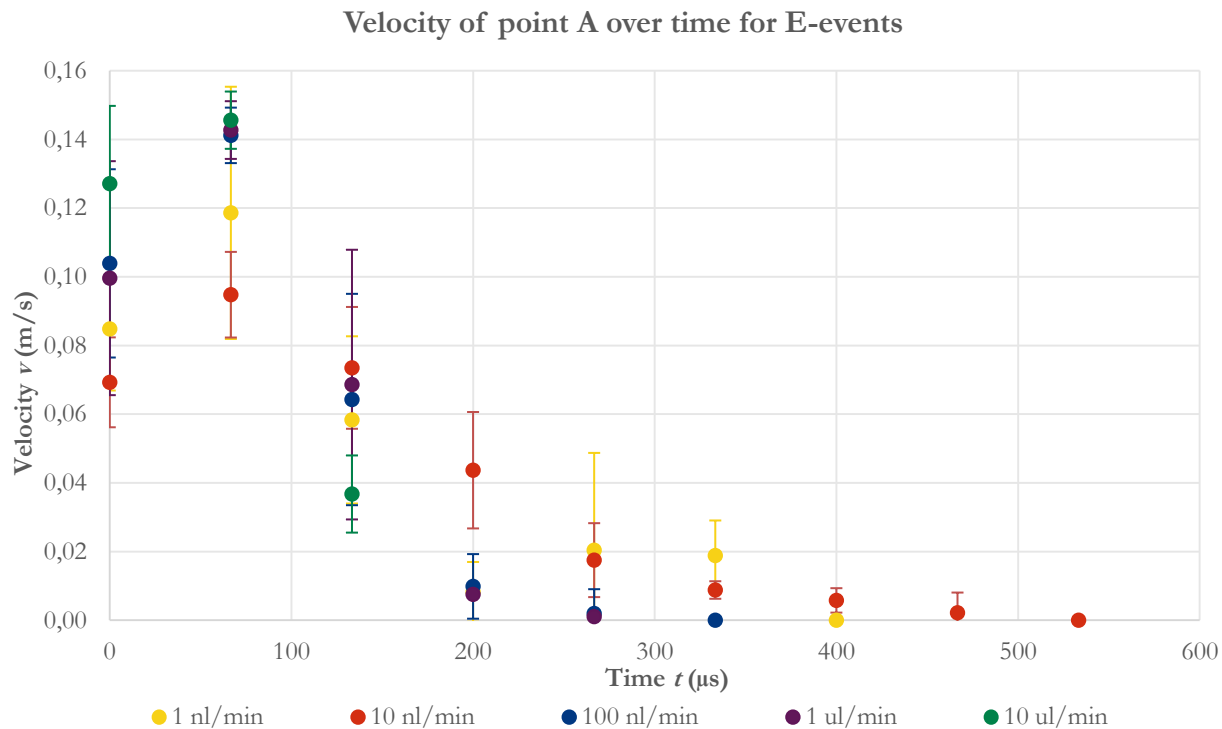


Figure C1. Velocity of point A over time for E-events for different flowrates.

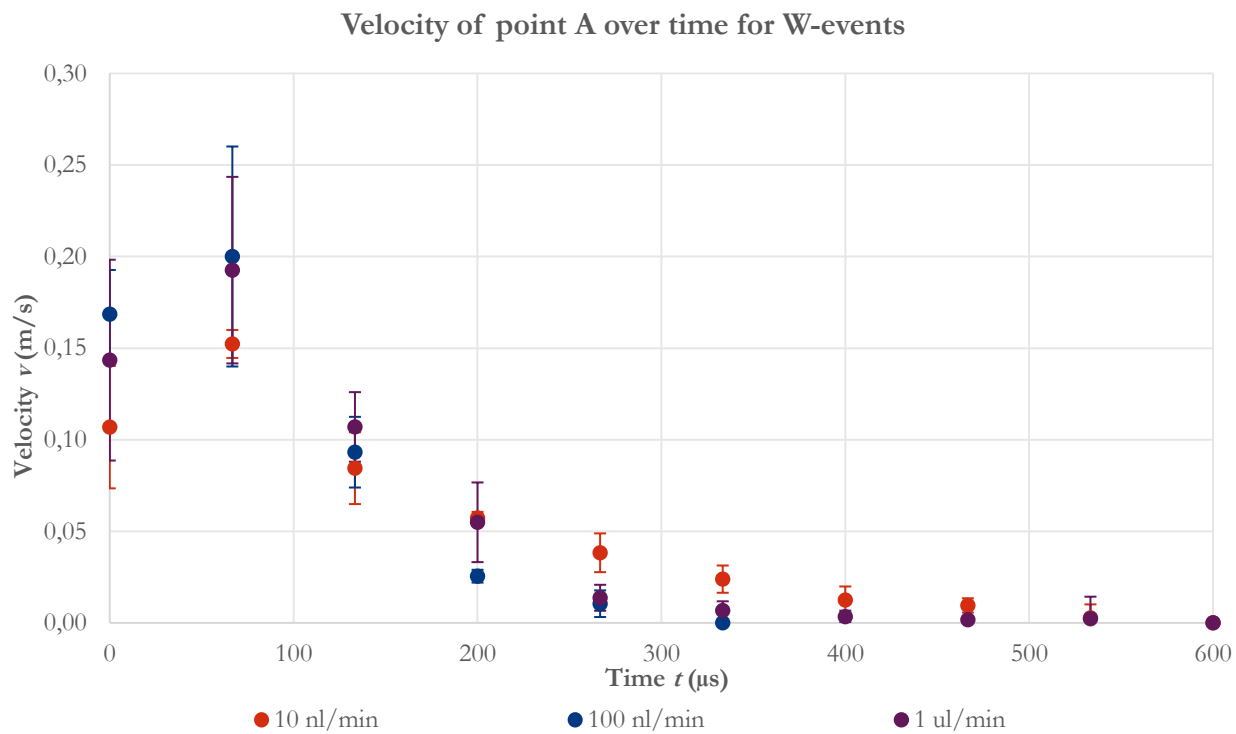


Figure C2. Velocity of point A over time for W-events for different flowrates.

Velocity of point B over time for C-events

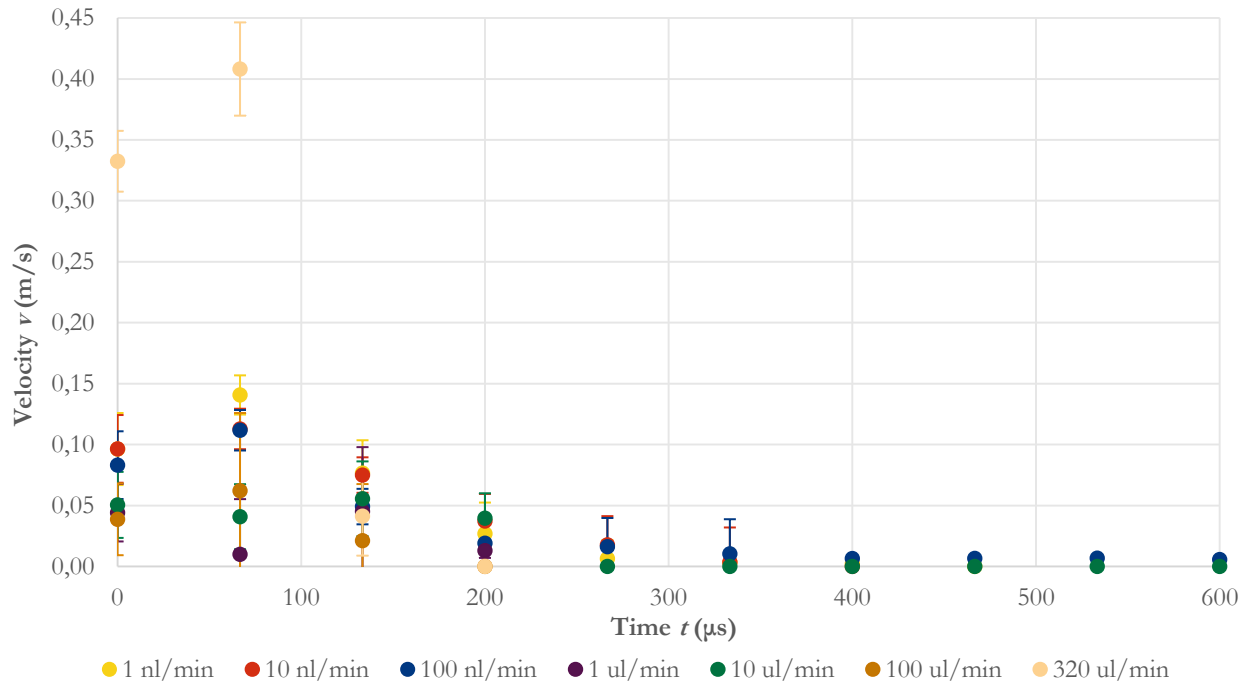


Figure C3. Velocity of point B over time for C-events.

Velocity of point over time B for E-events

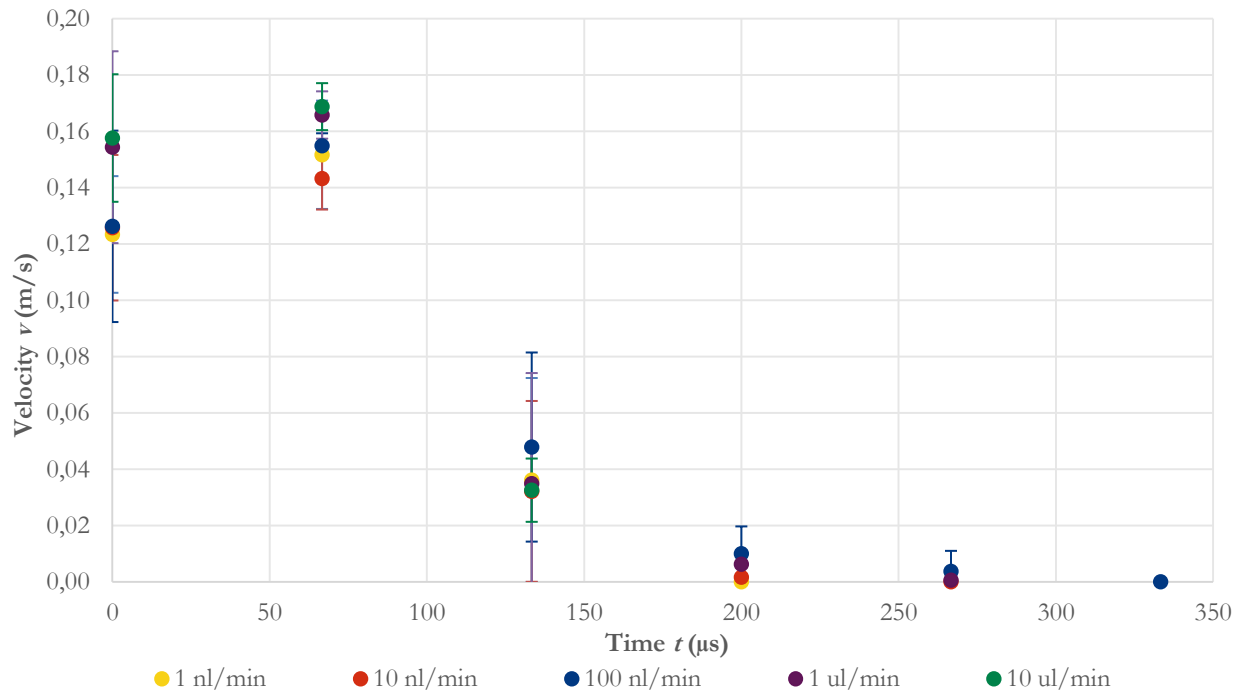


Figure C4. Velocities of point B over time for E-events.

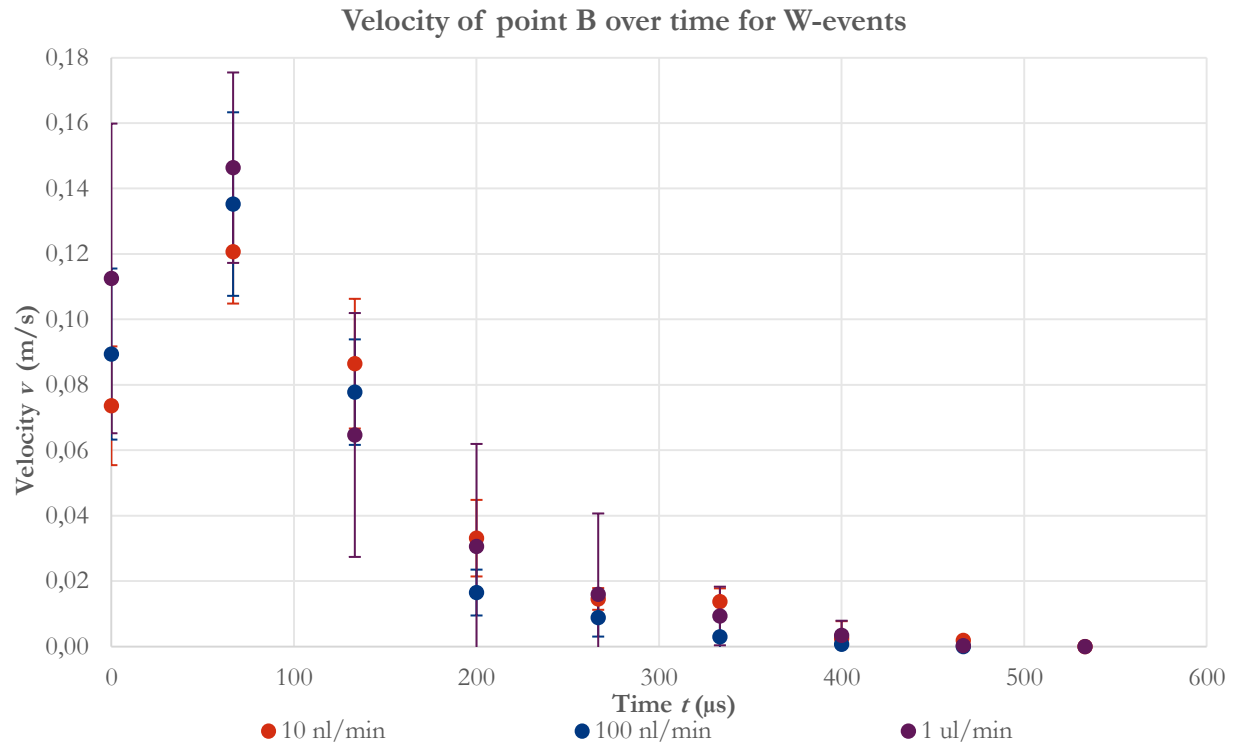


Figure C5. Velocities of point B over time for W-events.

## Appendix D: comparison interfacial velocity water-wet and intermediate-wet micromodel

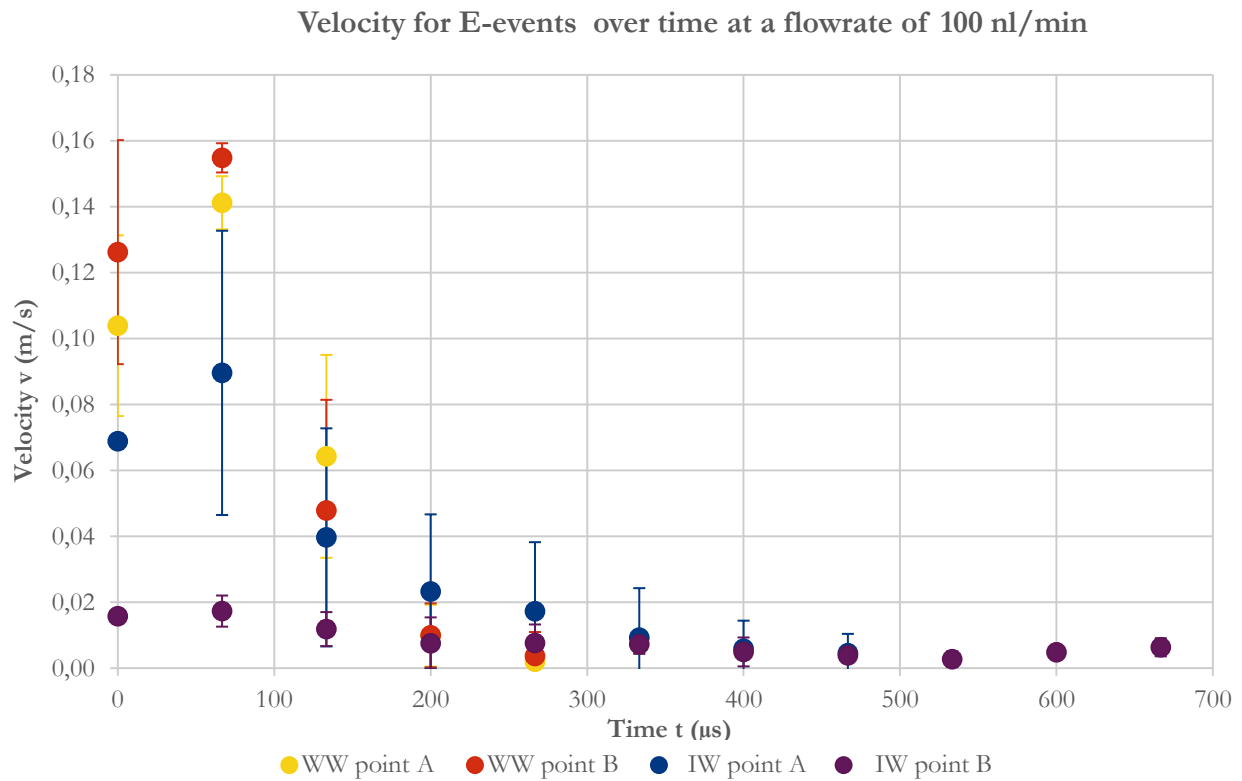


Figure D1. Comparison of the interfacial velocities for both intermediate-wet (IW) and water-wet (WW) micromodels.

## Appendix E: displacement front

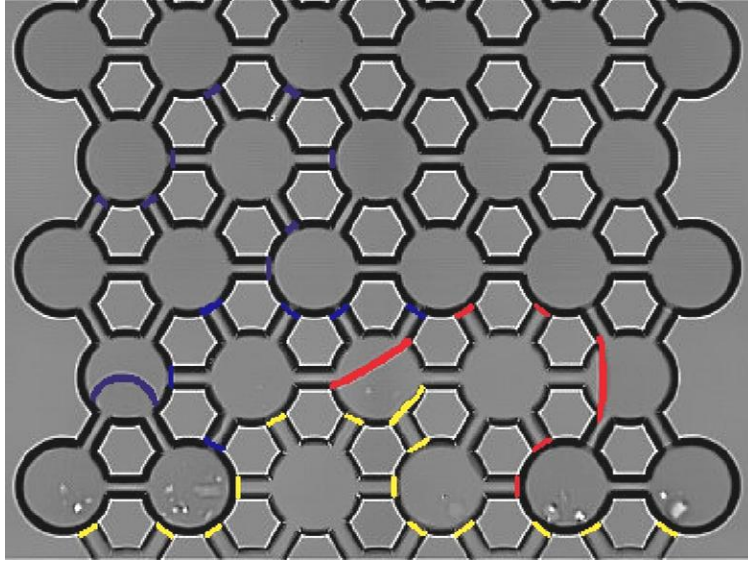


Figure E1. Displacement front at an injection flowrate of 1 nl/min. Time step is 91 ms.

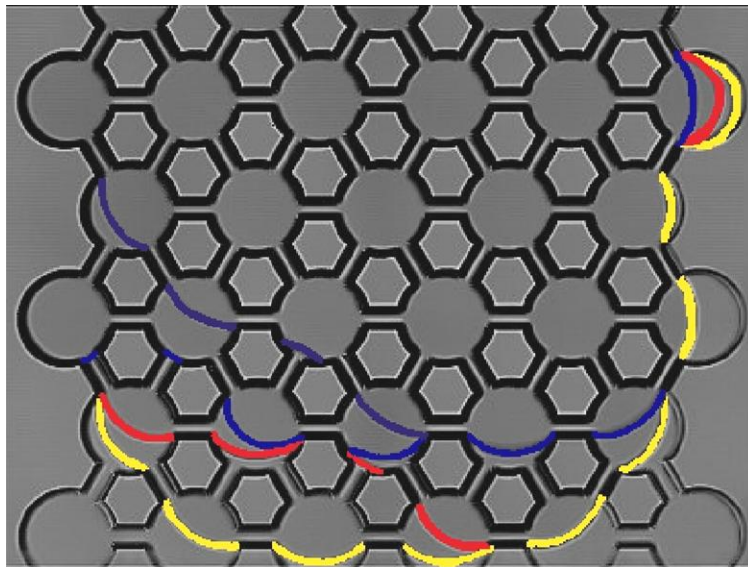


Figure E2. Displacement front at an injection flowrate of 10 nl/min. Time step is 424 ms.

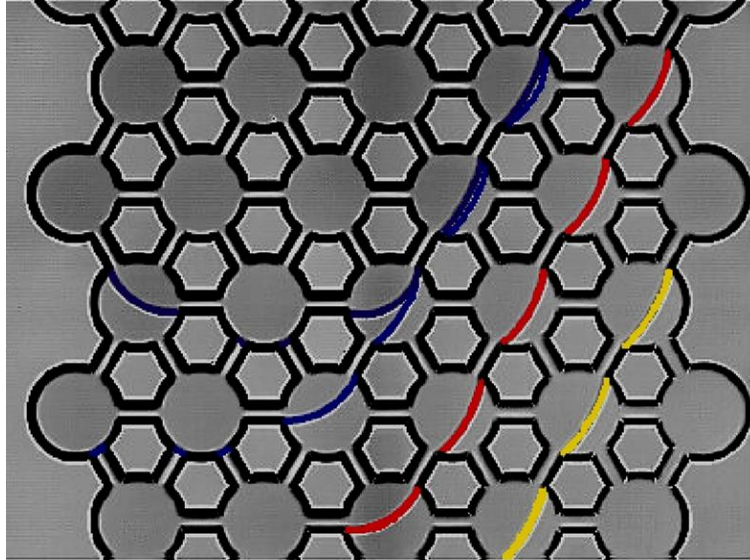


Figure E3. Displacement front at an injection flowrate of 100 nl/min. Time step is 690 ms.

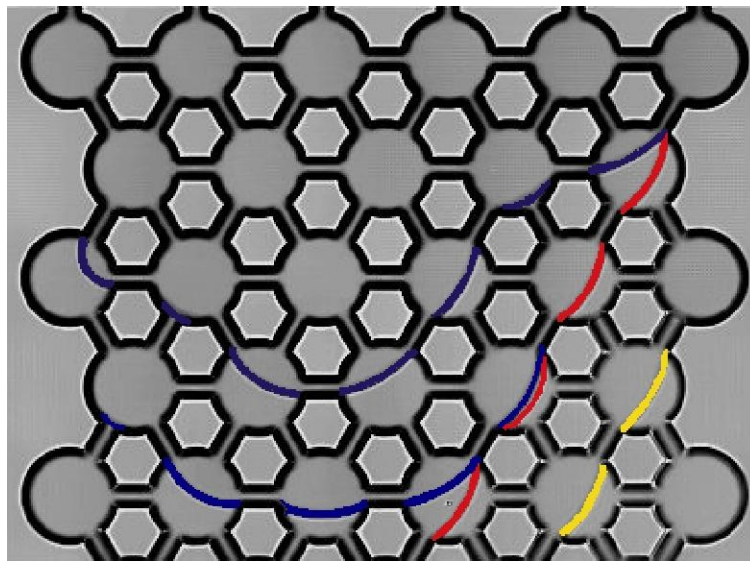


Figure E4. Displacement front at an injection flowrate of 1 µl/min. Time step is 40 ms.

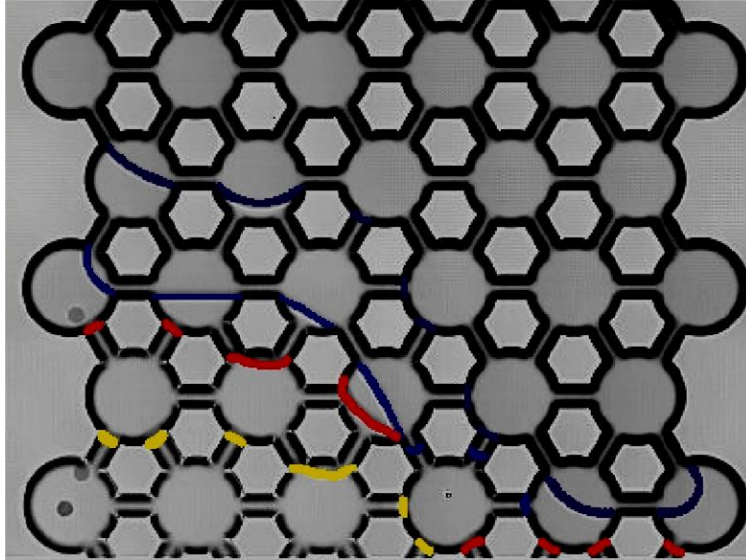


Figure E5. Displacement front at an injection flowrate of  $10 \mu\text{l}/\text{min}$ . Time step is 2,5 ms.

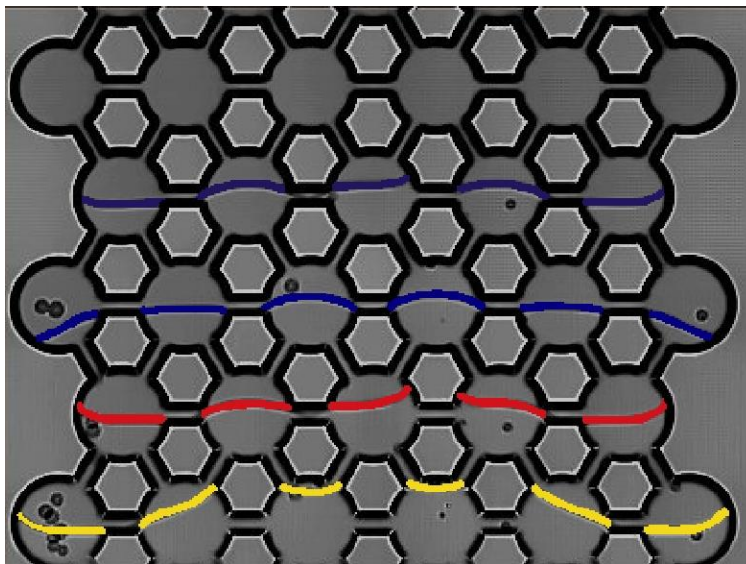


Figure E6. Displacement front at an injection flowrate of  $100 \mu\text{l}/\text{min}$ . Time step is 0,44 ms.

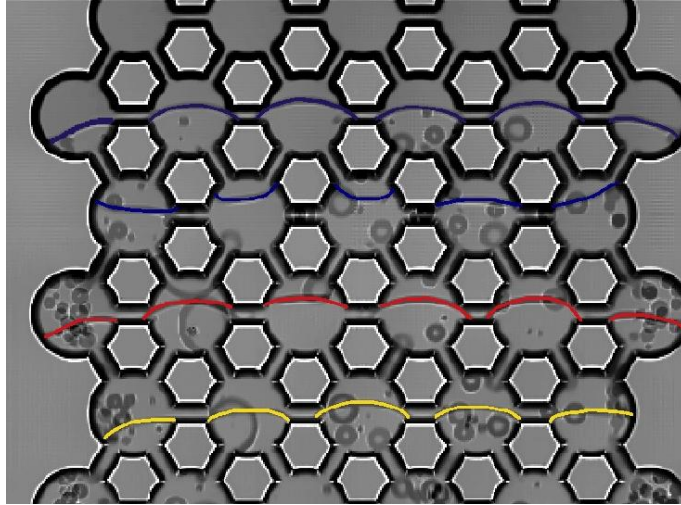


Figure E7. Displacement front at an injection flowrate of  $320 \mu\text{l}/\text{min}$ . Time step is  $0,24 \text{ ms}$ .

## Appendix F: original project description

Micromodel Imbibition Project

Advisor: Ryan Armstrong

Co-Advisor: Steffen Berg

### Background

Dynamic imbibition, often called water flooding, is a common secondary oil recovery practice, where a wetting phase (often water) is used to displace oil. Imbibition initially occurs at relatively high capillary pressure ( $P_c$ ), during which the wetting phase preferentially invades only the smallest pore-space regions. As  $P_c$  is decreased, progressively larger pore-space regions become saturated. However, due to variations in pore morphology, contact angle, interfacial tension, fluid viscosity, and flow rate, imbibition often lacks efficiency and a large fraction of non-wetting phase (i.e. oil) remains trapped in the pore-space. It is crucial to understand the physics of imbibition to increase oil recovery efficiency and to better understand many of constitutive relationships required for solving the flow equations used for reservoir simulation. Currently, there is a large interest in the oil and gas industry to model multiphase flow through porous media directly on 3D digital images of reservoir rock (this approach is often called “Digital Rock”) to de-risk and parameterize the large scale reservoir simulations. However, to validate our digital rock simulations experimental data is required. In particular, direct visual images of interfacial dynamics during imbibition are required to better understand the pore-scale mechanisms during oil displacement. One approach is to use micromodels which are a 2D representation of a porous media that allows for direct visualization of fluid motion via a transmission microscope.

### Imbibition

Water flooding inefficiency is explained by understanding the competition between viscous and capillary forces, which is critical since relative permeability, oil saturation, and oil blob morphology are directly dependent on the dominant force. To better understand this competition, Lenormand (1985) introduced the concept of a phase-diagram, where fluid displacement is characterized by two dimensionless numbers: capillary number and viscosity (or mobility) ratio. Capillary number is the ratio between viscous forces and capillary forces

$$N = \frac{v\mu}{\sigma}$$

where,  $v$  is the velocity (length per time) of the displacing phase,  $\mu$  is the viscosity (force multiplied by time per length squared) of the displacing phase, and  $\sigma$  the interfacial tension (force per length) between both phases. The viscosity ratio is the ratio between the viscosity of the displacing phase and the viscosity of the displaced phase

$$M = \frac{\mu_1}{\mu_2}$$

where,  $\mu_1$  is the viscosity of the displacing phase and  $\mu_2$  is the viscosity of the displaced phase.

The phase-diagram approach allows for the prediction of one of three displacement types: (1) capillary fingering, (2) viscous fingering, or (3) stable displacement, and thus, is a useful method for characterizing fluid displacement.

At the pore-scale (i.e. the length scale of a single pore), when capillary number is low (which often occurs during water flooding) the capillary force (i.e. interfacial forces) is dominant. During imbibition, as capillary pressure decreases, the wetting film (that covers the rock surface) thickness increases. At a critical capillary pressure the wetting film becomes too thick, and thus unstable, in the smallest most restricted pore-space regions (i.e. the pore throats). This instability causes the wetting film interface to collapse, which forces the adjoining non-wetting phase into an adjacent pore body. Depending on the number of surrounding pores saturated with wetting phase, the non-wetting phase may become disconnected from the bulk connected non-wetting phase and become trapped. This process often called “snap-off” (Figure 1a) is capillary controlled and is highly dynamic resulting in large interfacial velocities. Another capillary dominated process – Melrose Events (Figure 1b) – occurs when two separate interfaces converge in a single pore which leads to a capillary instability that rapidly advanced the interface through a pore. Both snap-off and Melrose events are pore-scale processes that lack direct experimental data. To gain a better understanding of these pore-scale processes the dynamics of these events need to be evaluated in porous systems to build conceptual mechanistic models.

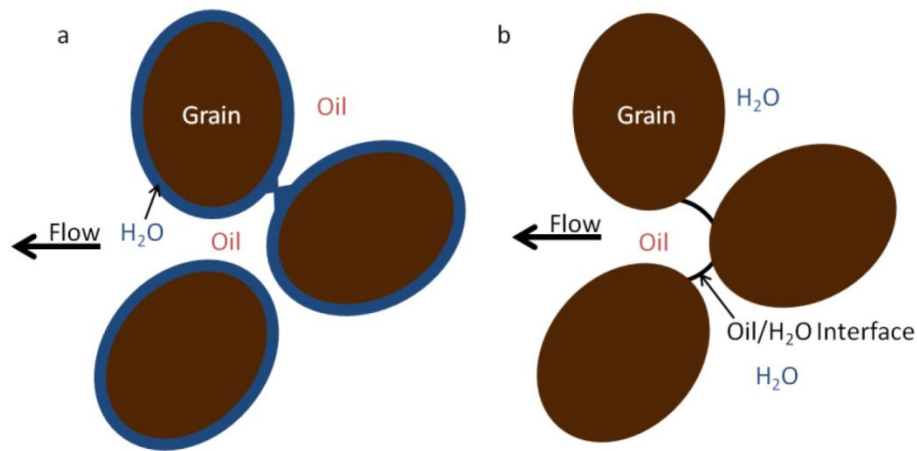


Figure F1. Snap-off occurring in the pore neck region (a) and Melrose event about to occur in the pore body region (b).

### Project Description

The project is an experimental study using a micro-fluidic device and transmission microscopy coupled with high speed photography to visualize pore-scale mechanisms during imbibition. The micro-fluidic device known as a “micromodel” consists of two glass plates chemically etched with a porous pattern and then bonded together, forming a porous network that can be visually inspected. *Experiments will be conducted to capture snap-off and Melrose events for a range of flow rates to evaluate the influence of viscous forces on these capillary dominated mechanisms.* Additionally, a limited amount of image processing will be done to measure interfacial velocities. Lastly, time permitting, a polymer solution will be added to the water phase to evaluate shear-rate dependent

viscosity effects during snap-off and Melrose events. The project will be embedded in a larger research and development team working on related subjects and directly supervised by two Shell researchers.

## Objectives

1. Produce pore-scale images of snap-off and Melrose events
2. Measure interfacial velocities using Open Source Physics Software
3. Evaluate if interfacial velocities are flow rate dependent (i.e. depend on pumping rate)
4. Redo objectives 1 through 3 using a polymer dissolved in the water phase
5. Measure polymer rheological properties with rheometer
6. Measure the polymers effective viscosity during immiscible displacement
7. Review literature on imbibition and create a report documenting the research
8. A successful project will include Objectives 1 through 3 and 7. However, completion of Objectives 1 through 7 will be encouraged – time permitting.

## Equipment

Transmission microscope, micromodels, rheometer, syringe pumps, and high speed camera are currently in-house. Additionally, there are numerous computers available for image processing.

For further questions please contact:

Ryan Armstrong

Rock and Fluid Science

Shell Global Solutions International BV

The Netherlands

[Ryan.Armstrong@Shell.com](mailto:Ryan.Armstrong@Shell.com)

070.447.4592